1521-009X/44/10/1584–1597$25.00
Drug Metabolism and Disposition
http://dx.doi.org/10.1124/dmd.116.070839
Drug Metab Dispos 44:1584–1597, October 2016

Cytochrome P450 3A4 and CYP3A5-Catalyzed Bioactivation of Lapatinib

Joanna K. Towles, Rebecca N. Clark, Michelle D. Wahlin, Vinita Uttamsingh, Allan E. Rettie, and Klarissa D. Jackson

Department of Pharmaceutical Sciences, Lipscomb University College of Pharmacy and Health Sciences. Nashville, Tennessee (J.K.T., R.N.C., K.D.J.); Department of Medicinal Chemistry, University of Washington School of Pharmacy, Seattle, Washington (M.D.W., A.E.R); and CoNCERT Pharmaceuticals, Inc., Lexington, Massachusetts (V.U.)

Received April 4, 2016; accepted July 21, 2016

ABSTRACT

Metabolic activation of the dual-tyrosine kinase inhibitor lapatinib by cytochromes CYP3A4 and CYP3A5 has been implicated in lapatinib-induced idiosyncratic hepatotoxicity; however, the relative enzyme contributions have not been established. The objective of this study was to examine the roles of CYP3A4 and CYP3A5 in lapatinib bioactivation leading to a reactive, potentially toxic quinoneimine. Reaction phenotyping experiments were performed using individual human recombinant P450 enzymes and P450-selective chemical inhibitors. Lapatinib metabolites and quinoneimine-glutathione (GSH) adducts were analyzed using liquid chromatography-tandem mass spectrometry. A screen of cDNA-expressed P450s confirmed that CYP3A4 and CYP3A5 are the primary enzymes responsible for quinoneimine-GSH adduct formation using lapatinib or *O*-dealkylated lapatinib as the substrate. The mean kinetic parameters (K_m and k_{cat}) of lapatinib *O*-dealkylation revealed that CYP3A4 was 5.2-fold more efficient than CYP3A5 at lapatinib *O*-dealkylation (CYP3A4 $k_{cat}/K_m = 6.8\ \mu M^{-1}\ min^{-1}$ versus CYP3A5 $k_{cat}/K_m = 1.3\ \mu M^{-1}\ min^{-1}$). Kinetic analysis of GSH adduct formation indicated that CYP3A4 was also 4-fold more efficient at quinoneimine-GSH adduct formation as measured by k_{cat} (maximum relative GSH adduct levels)/K_m (CYP3A4 = 0.0082 vs. CYP3A5 = 0.0021). In human liver microsomal (HLM) incubations, CYP3A4-selective inhibitors SR-9186 and CYP3cide reduced formation of GSH adducts by 78% and 72%, respectively, compared with >90% inhibition by the pan-CYP3A inhibitor ketoconazole. The 16%–22% difference between CYP3A- and CYP3A4-selective inhibition indicates the involvement of remaining CYP3A5 activity in generating reactive metabolites from lapatinib in pooled HLMs. Collectively, these findings support the conclusion that both CYP3A4 and CYP3A5 are quantitatively important contributors to lapatinib bioactivation.

Introduction

Lapatinib is an orally administered dual inhibitor of tyrosine kinases epidermal growth factor receptor 1 (EGFR) and human epidermal growth factor receptor 2 (HER2) (Rusnak et al., 2001; Lackey, 2006; Moy et al., 2007). EGFR and HER2 regulate downstream cell signaling pathways involved in cell growth, survival, and differentiation. Overexpression of HER2 is implicated in the pathogenesis of breast cancer (Yarden and Sliwkowski, 2001; Arteaga et al., 2012). Lapatinib (Tykerb) was first approved in 2007 for use in combination with capecitabine for the treatment of advanced or metastatic HER2-positive breast cancer in patients who are resistant to standard therapy with anthracycline, a taxane, and the HER2 monoclonal antibody trastuzumab (Geyer et al., 2006; Kopper, 2008). In addition, lapatinib, in combination with letrozole, is approved for the treatment of postmenopausal women with hormone receptor positive and HER2-positive advanced breast cancer for whom hormonal therapy is indicated (Johnston et al., 2009).

A mandatory black-box warning was released in 2008 for lapatinib-related hepatotoxicity owing to elevations in alanine aminotransferase (ALT) and aspartate aminotransferase observed in clinical trials and postmarketing surveillance; in rare cases, the liver injury was fatal (Tykerb product information: (http://www.accessdata.fda.gov/drugsatfda_docs/label/2010/022059s007lbl.pdf). Clinically significant ALT elevations have been reported in 1.6%–14.3% of patients receiving lapatinib (Moy et al., 2009; Azim et al., 2013). Lapatinib-induced hepatotoxicity is idiosyncratic in nature and is predominately hepatocellular; fewer cases of cholestasic or mixed liver injury have been reported (Spraggs et al., 2012). Evidence indicates that activation of the adaptive immune system is involved in liver injury associated with lapatinib (Spraggs et al., 2011; Parham et al., 2016); however, the underlying mechanisms remain unclear.

Previous reports suggest that metabolic activation of lapatinib to a chemically reactive metabolite may be a key initiating event in lapatinib-induced hepatotoxicity (Teng et al., 2010; Castellino et al., 2012; Spraggs et al., 2013). Lapatinib undergoes extensive metabolism by cytochromes P450 (P450) CYP3A4 and CYP3A5 and, to a lesser extent,

This research was supported by the National Institutes of Health National Cancer Institute [Grant K01CA190711]. Research reported in this publication is solely the responsibility of the authors and does not necessarily represent the official views of the National Institutes of Health.

dx.doi.org/10.1124/dmd.116.070839.

ABBREVIATIONS: ALT, alanine aminotransferase; DMSO, dimethylsulfoxide; EGFR, epidermal growth factor receptor 1; GSH, L-glutathione (reduced); HER2, human epidermal growth factor receptor 2; HLA, human leukocyte antigen; HLM, human liver microsome; HPLC, high-performance liquid chromatography; LAP-OH, *O*-dealkylated lapatinib; LC-MS/MS, liquid chromatography-tandem mass spectrometry; MRM, multiple reaction monitoring; *N*-dealkyl-LAP, *N*-dealkylated lapatinib primary amine; *N*-OH-LAP, *N*-hydroxylated lapatinib; Nrf2, nuclear factor erythroid 2-related factor 2; P450, cytochrome P450.

2C8, through three major routes: *O*-dealkylation, *N*-dealkylation, and *N*-hydroxylation (Fig. 1) (Takakusa et al., 2011; Castellino et al., 2012) plus some *C*-hydroxylation (Barbara et al., 2013). The *O*-dealkylated metabolite can be further oxidized to a reactive quinoneimine (Teng et al., 2010), which may covalently modify cellular proteins, potentially leading to cell stress and/or immune activation (Park et al., 2005). Both CYP3A4 and CYP3A5 have been shown to undergo mechanism-based inactivation by lapatinib (Teng et al., 2010; Chan et al., 2012); however, different reactive intermediates may be involved (Ho et al., 2015). Lapatinib is a quasi-irreversible inactivator of CYP3A4 through formation of a metabolic intermediate complex via a nitroso intermediate (Takakusa et al., 2011). In contrast, lapatinib may irreversibly inactivate CYP3A5 through covalent binding of the quinoneimine to the P450 apoprotein (Chan et al., 2012).

Although CYP3A4 and CYP3A5 are considered to be primarily responsible for lapatinib bioactivation, the relative contributions of each enzyme have not been well defined. CYP3A4 and CYP3A5 share 84% sequence similarity and display overlap in substrate specificity; however, they differ in expression and product regioselectivity (Aoyama et al., 1989; Wrighton et al., 1990; Gorski et al., 1994). CYP3A4 is the most abundantly expressed P450 in adult human liver and intestine (Shimada et al., 1994; Kolars et al., 1994; Guengerich, 1999), whereas CYP3A5 is highly polymorphic with significant interindividual variation in enzyme expression (Wrighton et al., 1990; Kuehl et al., 2001; Lamba et al., 2002). The major CYP3A5 variant allele is *CYP3A5*3*, and individuals who are homozygous for the *CYP3A5*3* allele (*CYP3A5*3/*3)* have low to undetectable levels of CYP3A5 protein compared with individuals who carry the *CYP3A5*1* "wild-type" allele (Kuehl et al., 2001; Lamba et al., 2002). The frequency of CYP3A5 expression (carriers of *CYP3A5*1* allele) is 10%–33% in the white population, 33% in Japanese, and 50–60% in African Americans (Kuehl et al., 2001; Lamba et al., 2002). CYP3A5 may account for greater than 50% of the total CYP3A content in *CYP3A5*1* carriers and may contribute significantly to the overall CYP3A activity in some cases (Kuehl et al., 2001; Lin et al., 2002).

Determining the roles of CYP3A4 and CYP3A5 in lapatinib bioactivation should improve understanding the clinical impact of CYP3A5 polymorphism on reactive metabolite generation and provide further insight into the factors that may influence individual risk for lapatinib-induced hepatotoxicity. Herein we have undertaken reaction phenotyping studies using human recombinant P450 enzymes and human liver microsomes (HLMs) in the presence of P450-selective inhibitors, including the CYP3A4-selective inhibitors SR-9186 and CYP3cide (Li et al., 2012; Walsky et al., 2012), to quantitatively

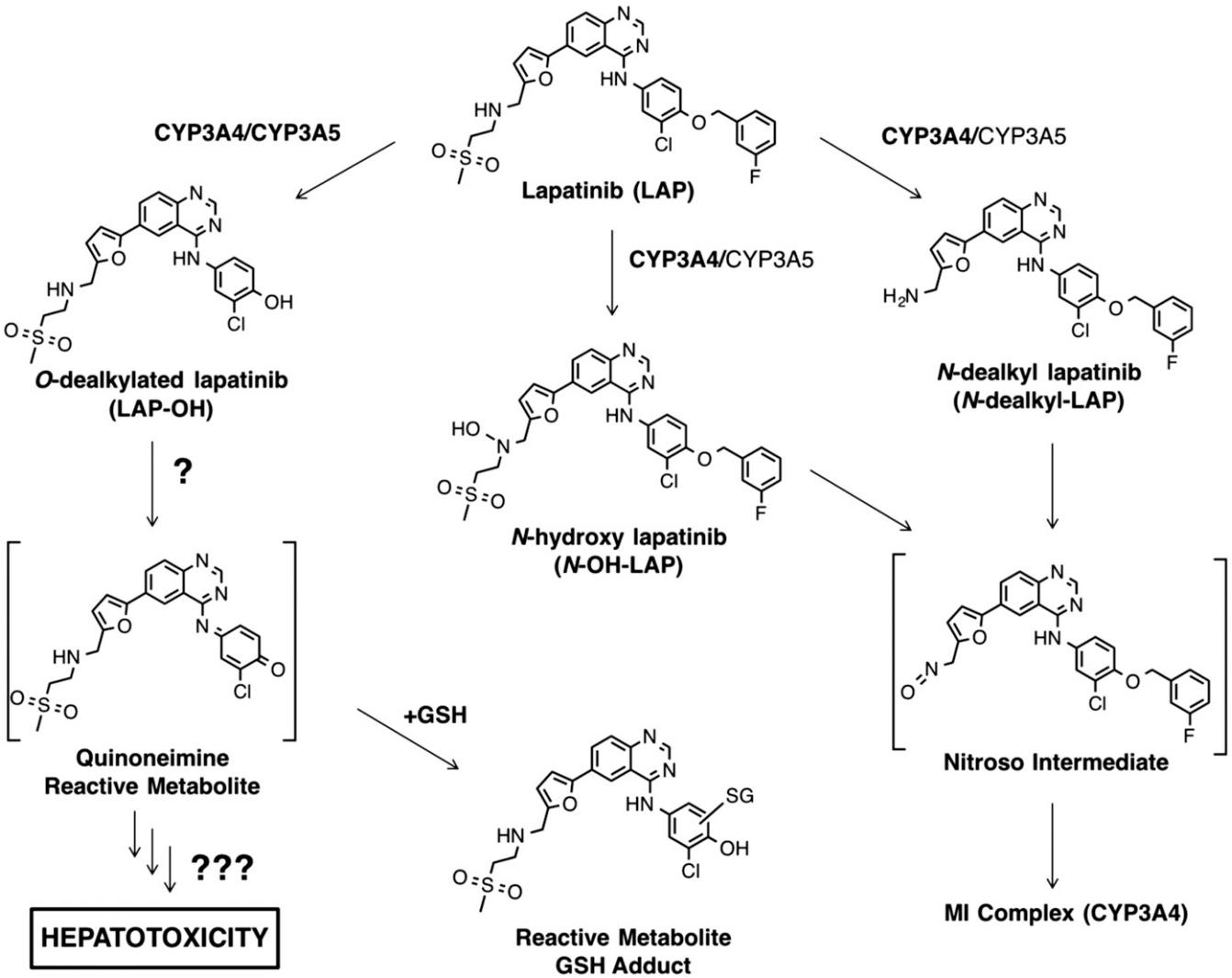

Fig. 1. Proposed metabolic pathway of lapatinib. (Adapted from Hardy et al., 2014.) MI, metabolic intermediate.

characterize the enzymatic contributions of CYP3A4 and CYP3A5 to lapatinib metabolism and bioactivation.

Materials and Methods

General Reagents

Lapatinib (free base) was purchased from LC Laboratories (Woburn, MA). The *O*-dealkylated metabolite of lapatinib (LAP-OH) was chemically synthesized from lapatinib as described previously (Teng et al., 2010). Deuterium-labeled standards of lapatinib ([$^2H_4$]lapatinib, d_4-lapatinib, C-20147) and *O*-dealkylated lapatinib ([$^2H_4$]*O*-dealkylated lapatinib, d_4-LAP-OH, C-10309) were provided by CoNCERT Pharmaceuticals (Lexington, MA) (Fig. 2). Stock solutions of lapatinib and LAP-OH were prepared in dimethylsulfoxide (DMSO). L-Glutathione (reduced, GSH) and chemical inhibitors α-naphthoflavone (7,8-benzoflavone), ticlopidine • HCl, sulfaphenazole, quinidine, 4-methylpyrazole • HCl, and ketoconazole were purchased from Sigma-Aldrich (St. Louis, MO). CYP3cide was purchased from Toronto Research Chemicals, Inc. (Toronto, ON, CAN), and SR-9186 was provided as a gift from Dr. Michael Cameron (Scripps Research Institute, Jupiter, FL). All other chemicals and reagents were of analytical grade and were purchased from standard commercial sources. Working solutions of lapatinib, LAP-OH, and chemical inhibitors were prepared from DMSO stocks, diluted into acetonitrile, to make up a solution in 1:9 DMSO/acetonitrile (v/v), unless otherwise stated.

Supersomes (baculovirus-infected insect cell microsomes) containing cDNA-expressed human CYP1A2, CYP2B6, CYP2C8, CYP2C9*1, CYP2C19, CYP2D6*1, CYP2E1, CYP3A4, and CYP3A5, coexpressed with P450 reductase and cytochrome b_5, except CYP1A2 and CYP2D6*1 (expressed without cytochrome b_5), were purchased from BD Biosciences or Corning Discovery Labware, Inc. (Woburn, MA). Pooled HLMs (150-Donor Ultra Pooled, mixed gender) were purchased from BD Biosciences or Corning Discovery Labware, Inc. In addition, pooled HLM fractions from 10 human liver samples (four males, five females, one unknown gender) provided by Dr. F. Peter Guengerich (Vanderbilt University) through the Tennessee Donor Services (Nashville, TN) were prepared according to a protocol previously described (Guengerich and Bartleson, 2008). An NADPH-regenerating system (solution A: 26 mM NADP+, 66 mM glucose 6-phosphate, 66 mM $MgCl_2$ in water; solution B: 40 U/ml glucose 6-phosphate dehydrogenase in 5 mM sodium citrate) was purchased from BD Biosciences or Corning Discovery Labware, Inc.

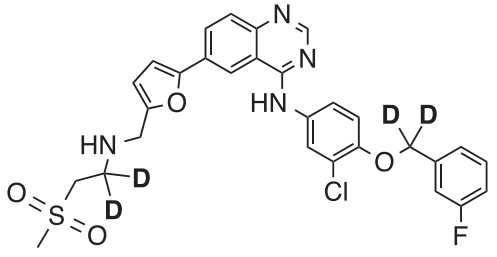

[$^2H_4$]lapatinib
(d_4-lapatinib, *C-20147*)

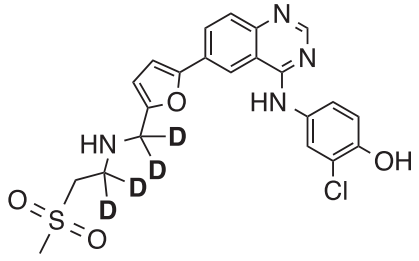

[$^2H_4$]*O*-dealkylated lapatinib
(d_4-LAP-OH, *C-10309*)

Fig. 2. Chemical structures of deuterium-labeled lapatinib and *O*-dealkylated lapatinib, internal standards. Compounds were synthesized by CoNCERT Pharmaceuticals, Inc.

Characterization of Deuterium-Labeled Analogs of Lapatinib and *O*-Dealkylated Lapatinib

Synthesis and characterization of deuterium-labeled analogs of lapatinib (d_4-lapatinib) and *O*-dealkylated lapatinib (d_4-LAP-OH) (structures shown in Fig. 2) were carried out by CoNCERT Pharmaceuticals. The mass spectral data and ^1H NMR data for d_4-lapatinib (C-20147, CoNCERT Pharmaceuticals, Inc.) were consistent with a fully deuterated d_4-lapatinib. In comparison with the NMR spectrum for d_0-lapatinib, in the C-20147 NMR spectrum, the –O-CH_2-signal was absent. The –NH-CH_2-signal was also absent, and the remaining -CH_2-SO_2-signal was collapsed to a singlet, indicating no hydrogens present on the adjacent position. D_4-LAP-OH (C-10309, CoNCERT Pharmaceuticals, Inc.) was prepared from the appropriate d_4-lapatinib (C-20076, *N*-(3-chloro-4-((3-fluorobenzyl)-oxy)phenyl)-6-(5-(((2-(methylsulfonyl)ethyl-1,1-d_2)amino)methyl-d_2)furan-2-yl)quinazolin-4-amine) by cleaving the unneeded fluorobenzyl moiety, and the deuterium composition present at the depicted sites did not change during the reaction. The mass spectral data and ^1H NMR data for the precursor C-20076 were consistent with significant deuteration at the two depicted sites. In comparison with the NMR spectrum for d_0-lapatinib, in the C-20076 NMR spectrum, the –NH-CH_2-CH_2- signal was absent, and the remaining -CH_2-SO_2- signal was collapsed to a singlet, indicating no hydrogens present on the adjacent position. Additionally, in the C-20076 NMR spectrum, the –NH_2-CH_2-furyl signal was present as a minor peak integrating to approximately 12% H, indicating approximately 88% D incorporation at that position.

Lapatinib Depletion by cDNA-Expressed CYP3A4 and CYP3A5

Lapatinib (1 μM) was incubated with human recombinant CYP3A4 and CYP3A5 enzymes (20 nM) in 0.10 M potassium phosphate buffer (pH 7.4). Incubations were prewarmed for 5 minutes in a shaking water bath at 37°C, and reactions were initiated by addition of the NADPH-regenerating system (final reaction volume, 1.0 ml; final concentration of organic solvent, 0.1% DMSO, 0.9% acetonitrile, v/v). Aliquots (100 μl) of the reaction mixture were removed at time points 0, 1, 2.5, 5, 10, 15, 20, 30, and 45 minutes and combined with an equal volume of ice-cold acetonitrile (containing 1 μg/ml of d_4-lapatinib, internal standard) to quench the reaction. The samples were mixed with a vortex device, placed on ice 5–10 minutes, and centrifuged (20 minutes at 20,000*g* at 4°C). The supernatants were analyzed by liquid chromatography-tandem mass spectrometry (LC-MS/MS) (method B, see *Analysis of Lapatinib and Metabolites by LC-MS/MS*) to measure relative levels of the remaining parent drug. Control incubations were performed without the NADPH-regenerating system. Two independent experiments were performed on separate days, and each experiment was conducted in triplicate. Similar results were obtained from both independent experiments. The data shown are from a single experiment conducted in triplicate on one day (n = 3).

Time-Course for Lapatinib Metabolite Formation

Lapatinib (5 μM) was incubated with human recombinant CYP3A4 and CYP3A5 (20 nM) in 0.10 M potassium phosphate buffer (pH 7.4). The time course of metabolite formation was examined in two separate experiments, one with shorter incubation times (0.5, 1, 2, and 5 minutes) and the second with longer incubation times (2, 5, 10, 20, and 30 minutes), each conducted in triplicate (n = 3), except at 30 minutes, which was in duplicate (n = 2) on the same day. Incubations were prewarmed for 5 minutes in a shaking water bath at 37°C, and reactions were initiated by the addition of the NADPH-regenerating system (final reaction volume, 1.0 ml; final concentration of organic solvent, 0.05% DMSO, 0.45% acetonitrile, v/v). At each time point, aliquots (100 μl) were removed and combined with an equal volume of ice-cold acetonitrile (containing 100 ng/ml of d_4-LAP-OH, internal standard) to quench the reaction. The sample was mixed with a vortex device, placed on ice 5–10 minutes, and centrifuged (20 minutes at 20,000*g* at 4°C). The supernatants were analyzed by LC-MS/MS (method A) to measure the relative levels of formation of the primary metabolites of lapatinib: *O*-dealkylated lapatinib (LAP-OH), *N*-dealkyl-lapatinib (*N*-dealkyl-LAP), and

N-hydroxy lapatinib (*N*-OH-LAP). Control incubations were without the NADPH-regenerating system. The data shown are the pooled data from the two experiments over the full time course (0.5, 1, 2, 5, 10, 20, and 30 minutes).

Relative Contributions of CYP Enzymes to Formation of Lapatinib Primary Metabolites and Reactive Metabolite-GSH Adducts

Lapatinib (5 μM) or LAP-OH (5 μM) was incubated with a panel of cDNA-expressed human P450 supersomes (CYP1A2, CYP2B6, CYP2C8, CYP2C9*1, CYP2C19, CYP2D6*1, CYP2E1, CYP3A4, and CYP3A5) (20 nM) in 0.10 M potassium phosphate buffer (pH 7.4) with and without supplementation with 5 mM GSH. Incubations were prewarmed for 5 minutes in a shaking water bath at 37°C. Reactions were initiated by addition of the NADPH-regenerating system (final reaction volume 200 μl) and continued for 2 minutes (without GSH) or 20 minutes (with GSH supplementation). For 2-minute incubations with lapatinib, the final concentration of organic solvent 0.1% DMSO, 0.9% acetonitrile, v/v. For 20-minute incubations with lapatinib, the final concentration of organic solvent 0.05% DMSO, 0.45% acetonitrile, v/v. After the incubation period, two volumes (400 μl) of ice-cold acetonitrile (containing 100 ng/ml of d_4-LAP-OH or d_4-lapatinib, internal standards) were added to quench the reaction. The sample was mixed with a vortex device, placed on ice 5–10 minutes, and centrifuged (20 minutes at 20,000*g* at 4°C). The supernatants were analyzed by LC-MS/MS (method A) to measure the relative levels of metabolite formation. To measure reactive metabolite-GSH adducts, the supernatants were dried under a gentle stream of nitrogen (N_2 gas) using a Biotage TurboVap system (Charlotte, NC) with water bath heated to 37°C for approximately 90 minutes. As much as possible, sample sets within a single experiment were dried for the same time period (~90 minutes) to ensure consistency. The remaining sample residue was redissolved in 100 μl of 3:7 acetonitrile/water (v/v), mixed with a vortex device, and centrifuged for 5 minutes. The supernatants were analyzed by LC-MS/MS (method A for incubations with LAP-OH and method C for incubations with lapatinib) to measure relative levels of metabolite formation. Control incubations were without the NADPH-regenerating system. For each condition tested, a single experiment was conducted in triplicate on 1 day (n = 3). For the 20-minute incubation with lapatinib, measurement of relative metabolite levels, including primary metabolites and reactive metabolite-GSH adducts, was determined from the same experiment.

Kinetic Assays with cDNA-Expressed CYP3A4 and CYP3A5

The kinetic parameters for lapatinib *O*-dealkylation and reactive quinoneimine-GSH adduct formation were determined using two to three different lots each of human recombinant CYP3A4 and CYP3A5 supersomes (BD Biosciences and Corning Discovery Labware, Inc.). The testosterone 6β-hydroxylase activity (marker of CYP3A activity) for each lot was measured by BD Biosciences and Corning Discovery Labware, Inc., and reported as follows: testosterone 6β-hydroxylase activities for CYP3A4 supersomes lots 3288855, 5224002, 5322004 were 170, 180, and 150 pmol product/(min × pmol P450), respectively; and testosterone 6β-hydroxylase activities for CYP3A5 Supersomes lots 4191001, 5258001, and 5350002 were 68, 49, 22 pmol product/(min × pmol P450), respectively. The reported NADPH-cytochrome c reductase activity ranged 2600–5200 nmol/(min × mg protein) between different enzyme lots (BD Biosciences and Corning Discovery Labware, Inc.).

Lapatinib *O*-Dealkylation. Lapatinib (0.1, 0.25, 0.5, 1.0, 2.5, 5.0, 10, 25, 50, and 100 μM) was incubated with 20 nM CYP3A4 supersomes (lots 5224002 and 5322004) and CYP3A5 supersomes (lots 5258001 and 5350002) for 2 minutes to determine the rates of LAP-OH formation. Preliminary experiments were conducted to determine the linearity of metabolite formation with respect to time and protein concentration. Reactions were initiated by the addition of the NADPH-regenerating system (final incubation volume, 200 μl; final concentration of organic solvent, 0.1% DMSO, 0.9% acetonitrile, v/v). After 2 minutes, reactions were terminated by the addition of an equal volume of ice-cold acetonitrile (containing 100 ng/ml d_4-LAP-OH). The samples were mixed with a vortex device and centrifuged (20 minutes at 20,000*g* at 4°C). The supernatants were analyzed by LC-MS/MS (method C) to measure LAP-OH formation. Two independent experiments each for CYP3A4 and CYP3A5 supersomes were performed. For each lot of enzyme, a single experiment was conducted in triplicate on 1 day (n = 3). Experiments with different lots of each enzyme were conducted and analyzed by LC-MS/MS on separate days. The pooled values (n = 6 for each enzyme) from the two experiments were used to determine the mean kinetic parameters (K_m, k_{cat}).

An authentic chemically synthesized standard of LAP-OH permitted the quantitation of LAP-OH formation using a standard curve. A 10-point standard curve was prepared by adding known concentrations of LAP-OH (final concentrations 1.0 ng/ml to 1000 ng/ml; final concentration of organic solvent, 0.1% DMSO, 0.9% acetonitrile, v/v) to 0.10 M potassium phosphate buffer (pH 7.4) with a mixture of heat-inactivated (boiled) CYP3A4 and CYP3A5 Supersomes (20 nM). This standard mix, prepared in duplicate for each concentration, was incubated for 2 minutes in a shaking water bath at 37°C, similar to the experimental samples; then an equal volume of ice-cold acetonitrile (containing 100 ng/ml d_4-LAP-OH) was added to each sample. The LAP-OH standards were prepared beforehand and stored at −20°C until LC-MS/MS analysis. For each day of LC-MS/MS analysis of the experimental samples from kinetic assays, the same LAP-OH standards were analyzed along with the experimental samples from day to day to assess inter-day variability.

Reactive Metabolite-GSH Adduct Formation. Lapatinib (0.1, 0.25, 0.5, 1.0, 2.5, 5.0, 10, 25, 50, and 100 μM) was incubated with 20 nM CYP3A4 Supersomes (lots no. 3288855, 5224002, and 5322004) and CYP3A5 supersomes (lots 4191001, 5258001, and 5350002) supplemented with 5 mM GSH and the NADPH-regenerating system for 20 minutes to determine the relative rates of reactive quinoneimine-GSH adduct formation. Preliminary experiments were conducted to determine the linearity of reactive metabolite-GSH adduct formation with respect to time and protein concentration. Reactions were initiated by the addition of the NADPH-regenerating system (final incubation volume 200 μl; final concentration of organic solvent, 0.1% DMSO, 0.9% acetonitrile, v/v). After 20 minutes, reactions were terminated by addition of two volumes of ice-cold acetonitrile (containing 100 ng/ml d_4-LAP-OH). The samples were mixed with a vortex device and centrifuged (20 minutes at 20,000*g* at 4°C). The supernatants were dried under a gentle stream of nitrogen for approximately 90 minutes using a Biotage TurboVap system (Charlotte, NC) with a heated water bath at 37°C. The remaining sample residue was redissolved in 100 μl of 3:7 acetonitrile/water (v/v), mixed with a vortex device, and centrifuged for 5 minutes. The supernatants were analyzed by LC-MS/MS (method C) to measure relative levels of metabolite formation. The ratio of peak areas for GSH adducts to internal standard were calculated to provide a relative measurement of metabolite formation because an authentic chemical standard of the quinoneimine-GSH adduct was not available. Independent experiments with three different lots each of CYP3A4 and CYP3A5 supersomes were performed on separate days. For each lot of enzyme (CYP3A4 lots 3288855 and 5224002; CYP3A5 lots 4191001 and 5258001), a single experiment was conducted in duplicate or triplicate on 1 day (n = 2 to 3). Experiments with one lot of CYP3A4 and one lot of CYP3A5 supersomes each were conducted and analyzed by LC-MS/MS on the same day for comparison. For CYP3A4 lot 5322004 and CYP3A5 lot 5350002, two and three independent experiments for each lot, respectively, were conducted in triplicate and analyzed by LC-MS/MS on separate days to evaluate interday variability. The combined values (n = 11 for each enzyme) from four independent experiments were pooled to determine the mean kinetic parameters, apparent K_m and k_{cat} (maximum relative GSH levels, peak area ratio). When determining relative levels of GSH adducts, a standard sample of d_4-LAP-OH was run each day at the beginning, middle, and end of the LC-MS/MS sequence to evaluate intraday consistency of the LC-MS/MS signal.

Effect of P450 Chemical Inhibitors on Lapatinib Metabolite Formation

Lapatinib (5 μM) or LAP-OH (5 μM) was incubated with 150-donor pooled HLMs (0.1 mg/ml) supplemented with 5 mM GSH in the presence of P450-selective chemical inhibitors to determine the effect on metabolite formation. The following chemical inhibitors were used to block the respective P450: α-naphthoflavone (1 μM, CYP1A2), ticlopidine (5 μM, CYP2B6 and CYP2C19), sulfaphenazole (5 μM, CYP2C9), quinidine (2 μM, CYP2D6), 4-methylpyrazole (100 μM, CYP2E1), and ketoconazole (1 μM, CYP3A). Control incubations were carried out with vehicle (1:9 DMSO/acetonitrile, v/v) in the absence of inhibitor. The final concentration of organic solvent for each incubation was 0.1% DMSO, 0.9% acetonitrile (v/v). Reactions were initiated by the addition of the NADPH-regenerating system (final reaction volume, 200 μl) and continued for 20 minutes. After the incubation period, reactions were quenched by the addition of two volumes (400 μl) of ice-cold acetonitrile (containing 100 ng/ml of

d_4-lapatinib, internal standard) to quench the reaction. Samples were prepared as described above. Relative levels of lapatinib metabolites and GSH adducts were measured by LC-MS/MS (method C) and compared with vehicle control incubations without inhibitor. The percent control of GSH adduct formation was calculated relative to vehicle control incubations with no inhibitor. For incubations with lapatinib, a single experiment was conducted in triplicate on 1 day ($n = 3$). For incubations with LAP-OH, two independent experiments were performed on two separate days, and each experiment was conducted in triplicate. The combined data from both experiments are shown ($n = 6$).

Effect of CYP3A4-Selective Inhibitors on Lapatinib Metabolite Formation

In a separate series of experiments, the CYP3A4-selective inhibitors SR-9186 (Li et al., 2012) and CYP3cide (Walsky et al., 2012) were used to distinguish the roles of CYP3A4 versus CYP3A5 in lapatinib metabolism. SR-9186 is a competitive CYP3A4 inhibitor (Li et al., 2012), and CYP3cide is a time-dependent CYP3A4 inactivator. Ketoconazole was used as a competitive pan-CYP3A inhibitor to establish baseline CYP3A contribution. For experiments with SR-9186, working solutions of the inhibitor were prepared in 1:9 DMSO/acetonitrile (v/v), and reactions were carried out in glass vials to prevent compound binding to plastic (Li et al., 2012). Lapatinib (5 μM) was incubated with 10-donor pooled human liver microsomes (0.1 mg protein/ml), 5 mM GSH in the presence of SR-9186 (2.5 μM), ketoconazole (1 μM), or vehicle (1:9 DMSO/acetonitrile). The final concentration of organic solvent for each incubation was 0.1% DMSO, 0.9% acetonitrile (v/v). Reactions were initiated by the addition of the NADPH-regenerating system (final reaction volume, 200 μl). After a 20-minute incubation, reactions were quenched by the addition of two volumes (400 μl) of ice-cold acetonitrile (containing 100 ng/ml of d_4-lapatinib, internal standard). Sample preparation was similar to that described here. Relative levels of reactive metabolite-GSH adducts were measured by LC-MS/MS (method C) analysis. The percent control GSH adduct formation was calculated relative to vehicle control incubations with no inhibitor. A single experiment was conducted in triplicate on one day ($n = 3$).

Experiments with CYP3cide involved a two-step time-dependent inactivation procedure, similar to that described by Walsky et al. (2012). Briefly, the primary incubation contained CYP3cide (0.5 μM, diluted from 10 μM solution in 1:10 methanol/water) or vehicle (1:10 methanol/water, v/v) with 10-donor or 150-donor pooled HLMs (final concentration, 1.0 mg protein/ml) in 0.10 M potassium phosphate buffer (pH 7.4). The inactivation mixture was prewarmed for 5 minutes, and the reaction was initiated by the addition of the NADPH-regenerating system (final reaction volume, 100 μl; final organic solvent, 0.5% methanol). After a 5-minute incubation, a 20-μl aliquot of the primary reaction mixture was diluted 1:10 into a secondary reaction mixture containing 5 μM lapatinib, the NADPH regenerating system, and 5 mM GSH with or without ketoconazole (1 μM final concentration; diluted from 200 μM solution in acetonitrile). The final volume of the secondary incubation was 200 μl, with a final protein concentration of 0.1 mg protein/ml. The final concentration of organic solvent for the secondary incubation was 0.05% DMSO, 0.95% acetonitrile, and 0.05% methanol (v/v/v). The secondary reaction was allowed to proceed for 20 minutes. Reactions were quenched by the addition of two volumes (400 μl) of ice-cold acetonitrile (containing 100 ng/ml of d_4-lapatinib or 100 ng/ml of d_4-*O*-dealkylated lapatinib, internal standards). The relative levels of reactive metabolite-GSH adduct formation were measured by LC-MS/MS (method C) analysis and compared with vehicle control incubations. For incubations with CYP3cide, two independent experiments were performed on 2 separate days. The first experiment was carried out using 10-donor pooled HLMs, and the second experiment was repeated with 150-donor pooled HLMs. Each experiment was conducted in triplicate. The data shown for CYP3cide are compiled from the two independent experiments ($n = 6$).

Analysis of Lapatinib and Metabolites by LC-MS/MS

LC-MS/MS Method A. A Waters Micromass Quattro Micro II triple quadrupole mass spectrometer (Waters Corporation, Milford, MA) coupled to two Shimadzu LC-10AD pumps with a gradient controller and a Shimazdu SIL-10ADvp autoinjector (Shimadzu, Columbia, MD) was used at the University of Washington School of Pharmacy, Mass Spectrometry Center for the analysis of lapatinib and its metabolites. A 30-μl aliquot of each sample was injected into the equilibrated high-performance liquid chromatography (HPLC) system. Solvents A and B were Optima LC/MS-grade water (Fisher Scientific, Pittsburg, PA) with 0.1% (v/v) trifluoroacetic acid and Optima LC/MS-grade acetonitrile (Fisher Scientific, Pittsburgh, PA) with 0.1% (v/v) trifluoroacetic acid, respectively. Analyte separation was achieved with an Agilent Zorbax SB-C18 column (5 μm, 150 mm $\times$ 2.1 mm) (Agilent Technologies, Santa Clara, CA) at a flow rate of 0.3 ml/min. The gradient program was as follows: 15% B (0–1.0 minute), linear gradient from 5% to 95% B (1.0–4.5 minutes), 95% B (4.5–6.0 minutes), and returned to 5% B (7.10–8.0 minutes) (all v/v). The total run time was 8 minutes. The eluent was introduced directly into the mass spectrometer via electrospray ionization in positive ion mode. The MS spectral data were analyzed and deconvoluted using MassLynx version 4.1 (Waters Corporation, Milford, MA).

LC-MS/MS Methods B and C. A Thermo TSQ Quantum Triple Quadrupole mass spectrometer (Thermo Fisher Scientific, Waltham, MA) interfaced with an HPLC system and a Thermo PAL autoinjection system was used at the Lipscomb University College of Pharmacy, Pharmaceutical Sciences Bioanalytical Core, for analysis of lapatinib and its metabolites. A 20-μl aliquot of each sample was injected into the equilibrated HPLC column. Solvents A and B were Optima LC/MS-grade water (Fisher Scientific) with 0.1% (v/v) formic acid and Optima LC/MS-grade acetonitrile (Fisher Scientific) with 0.1% (v/v) formic acid, respectively. Two HPLC methods were used for analyte separation with different C18 columns and gradient programs. Method B used an Agilent Zorbax SB-C18 column (5 μm, 150 mm $\times$ 2.1 mm) (Agilent Technologies, Santa Clara, CA) with a flow rate of 0.3 ml/min and column oven temperature of 30°C. The gradient program was as follows: 15% B (0–1.0 minutes), linear gradient from 5% to 95% B (1.0–4.5 minutes), 95% B (4.5–6.0 minutes), and returned to 5% B (7.10–8.0 minutes) (all v/v). Method C used a Kinetex C18 or EVO C18 column (2.6 μm, 50 mm $\times$ 2.1 mm, 100 Å) (Phenomenex Inc., Torrance, CA) with a flow rate of 0.3 ml/min and a column oven temperature of 30°C. The gradient program for analysis of lapatinib and its metabolites was as follows: 5% B (0–1.0 minute), linear gradient from 5% to 95% B (1.0–3.5 minutes), 95% B (4.0–4.5 minutes), and returned to 5% B (4.5–5.0 minutes) (all v/v). This latter method provided a shorter run time (5 minutes) while maintaining analyte separation. For both methods, the eluent was introduced directly into the mass spectrometer via electrospray ionization in positive ion mode. The MS spectral data were analyzed and deconvoluted using Thermo Xcalibur software 2.0 (Thermo Fisher Scientific, Waltham, MA).

Detection and Quantitation of Lapatinib and Metabolites

For each LC-MS/MS method described here, lapatinib and its metabolites were selectively detected using multiple (selected) reaction monitoring (MRM). The following precursors to product MRM transitions were used for the detection of lapatinib and lapatinib metabolites based on structurally specific fragmentation obtained from collision-induced dissociation with collision energy 18–30 V: m/z 581.6 $\rightarrow$ 365 for lapatinib, m/z 473 $\rightarrow$ 350 for *O*-dealkylated lapatinib (LAP-OH); m/z 475 $\rightarrow$ 366 for *N*-dealkyl lapatinib (*N*-dealkyl-LAP), m/z 597 $\rightarrow$ 458 for *N*-hydroxy lapatinib (*N*-OH-LAP), and m/z 778 $\rightarrow$ 655 for quinoneimine-GSH adducts, as previously described (Hardy et al., 2014). The MRM transitions for stable isotope-labeled internal standards were: d_4-lapatinib m/z 585 $\rightarrow$ 365, and d_4-LAP-OH m/z 477 $\rightarrow$ 352. (Fig. 3). The retention time for LC-MS/MS peaks varied slightly from day to day (e.g., lapatinib retention time on one day was 2.37 minutes, and on another day, the retention time was 2.56 minutes (Fig. 3, A and B); however, this may be due to slight variations in mobile phase composition, and so forth. Peak areas for each analyte were determined using the peak detection (autointegration) function in Thermo Xcalibur or MassLynx software. The MRM peak area ratio corresponding to the drug/metabolite analyte peak area over the internal standard peak area was used for quantitative and semiquantitative analysis of lapatinib and metabolites.

Data Analysis

Substrate depletion data for recombinant CYP3A4 and CYP3A5 were fitted to biexponential (two-phase) and monoexponential (one-phase) decay models, respectively, through nonlinear regression analysis using GraphPad Prism 6 (GraphPad Software Inc., San Diego, CA). All experiments were performed with three replicate samples (triplicate) unless otherwise stated. Data presented are means $\pm$ S.D. unless otherwise stated. The rate constants (k, k_{fast}, and k_{slow}) were estimated using GraphPad Prism 6 software to determine the relative rates of lapatinib depletion by metabolism. Goodness of fit was assessed by the R^2 value

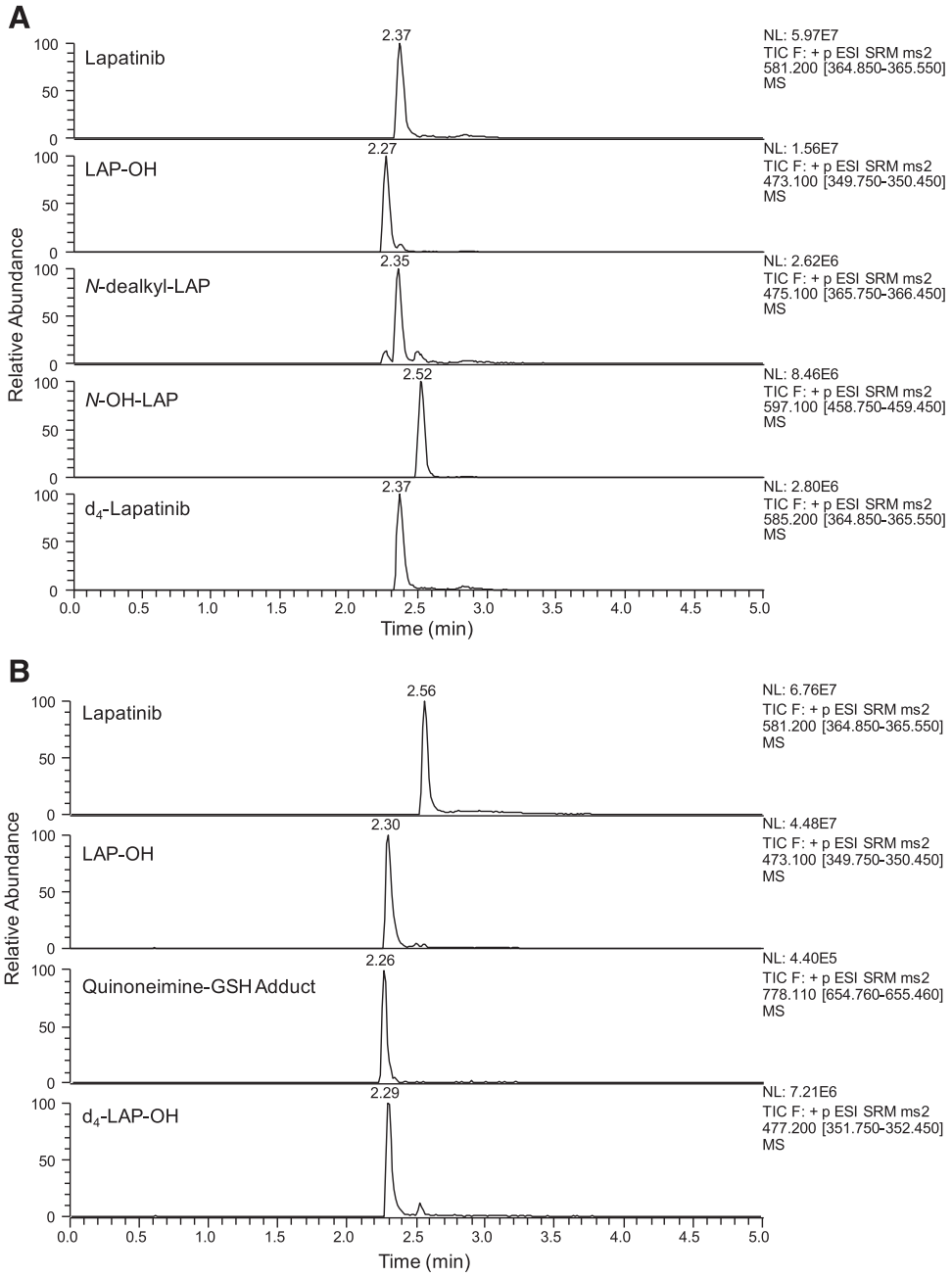

Fig. 3. Representative LC-MS/MS chromatograms from analysis of lapatinib and lapatinib metabolites. Selected/MRM was used for the detection of lapatinib and its metabolites. The specific precursor to product transitions for parent drug, metabolites, and internal standards are shown. (A) MRM analysis with d_4-lapatinib as the internal standard. (B) MRM analysis with d_4-LAP-OH as the internal standard. Peak areas were determined using the peak detection (autointegration) function in Thermo Xcalibur Qual Browser software (Thermo Fisher Scientific, Waltham, MA).

and visual examination of the data. Kinetic assays for lapatinib *O*-dealkylation and reactive metabolite-GSH adduct formation were carried out with two independent experiments (for LAP-OH) or four independent experiments (for GSH adducts), and each experiment was conducted in duplicate or triplicate ($n = 2$ or 3). Standard curve fitting for LAP-OH quantitation was accomplished by linear regression analysis (LAP-OH/d_4-LAP-OH peak area ratio versus LAP-OH concentration) using Microsoft Excel. Similar results for the standard curve were obtained on each day of LC-MS/MS analysis. Because an analytical standard of the quinoneimine-GSH adduct was not available to quantify the rate of product formation, the maximum relative GSH adduct levels were estimated based on the LC-MRM peak area ratio. Peak area ratio was calculated by determining the ratio of GSH adduct peak area to d_4-LAP-OH internal standard peak area (GSH adduct/d_4-LAP-OH).

Eadie-Hofstee plots (velocity versus velocity/[S]) were constructed to determine whether the kinetic profiles for LAP-OH and GSH adduct formation followed the Michaelis-Menten model (Houston and Kenworthy, 2000; Hutzler and Tracy, 2002; Atkins, 2005). Visual examination of the data for CYP3A4 and CYP3A5 indicated linear relationships between metabolite formation rate and rate/substrate concentration (except at the lowest substrate concentrations, in which sensitivity of metabolite detection was low). Curve fit was evaluated using Akaike's Information Criterion and extra sum-of-squares *F* test from nonlinear regression analysis in GraphPad Prism 6 to select the "best-fit" model (Ramirez et al., 2004; Vuppugalla and Mehvar, 2005). Kinetic profiles for CYP3A4 and CYP3A5 were compared between the Michaelis-Menten, substrate inhibition, and two-site binding models. In each case, the Michaelis-Menten equation was the preferred model. Thus, kinetic data were fit to the Michaelis-Menten equation, and the mean K_m and k_{cat} values were determined using nonlinear regression analysis with GraphPad Prism 6. Apparent K_m and k_{cat} values were expressed as mean ± S.E.M.). The kinetic profiles generated from each substrate saturation experiment were compared using an extra sum-of-squares F test (GraphPad Prism 6) to evaluate interday and intraday variability as well as to compare kinetic parameters from lot-to-lot of recombinant enzymes. Grubbs' test ($\alpha = 0.05$) for outlier detection (GraphPad Prism 6 software) was used to identify outliers in the data sets

obtained from repeated kinetic assays. The mean kinetic parameters (K_m and k_{cat}) from LAP-OH and GSH adduct formation were compared between CYP3A4 versus CYP3A5 supersomes using an unpaired two-tailed *t* test. The mean values from chemical inhibition experiments with pooled HLMs were compared with control incubations without inhibitor or to incubations with other inhibitors using an unpaired two-tailed *t* test. Correlation analysis was performed using the Pearson *r* correlation test in GraphPad Prism to compare enzyme activities by enzyme lots with the kinetic parameters of GSH adduct formation (relative k_{cat}/K_m). Statistical significance was established as $P < 0.05$.

Results

Lapatinib Substrate Depletion by CYP3A4 and CYP3A5. The depletion of lapatinib over time by human recombinant CYP3A4 and CYP3A5 was determined to estimate the relative effectiveness of each enzyme in the overall metabolism of lapatinib. In the log-transformed data, two phases were readily apparent in the depletion profile for CYP3A4 but not with CYP3A5 (Fig. 4, A and B). In the initial phase of incubations, the estimated rate constant for lapatinib metabolism by CYP3A4 was $k_{fast} = 2.1 \pm 0.53$ minute^{-1} compared with $k = 0.1 \pm 0.01$ minute^{-1} for CYP3A5. Thus, CYP3A4 was approximately 21-times faster than CYP3A5 in the overall metabolism of lapatinib during this initial phase. Over time, however, the rate of metabolism by CYP3A4 markedly decreased (CYP3A4 $k_{slow} = 0.2 \pm 0.06$ minute^{-1}).

Lapatinib Metabolite Formation by CYP3A4 and CYP3A5. Next, the formation of the primary metabolites of lapatinib by CYP3A4 and CYP3A5 was monitored over time to better understand the kinetics of metabolite generation. The concentration of lapatinib (5 μM) used for these studies was selected because it is within the therapeutic range of the drug; the reported peak plasma concentration ($C_{p,max}$) after a 1250-mg daily dose of lapatinib was 4.2 μM (2.4 μg/ml) (range, 2.7–6.5 μM) (Tykerb product information; http://www.accessdata.fda.gov/drugsatfda_docs/label/2010/022059s007lbl.pdf). The primary metabolites monitored herein were products of lapatinib *O*-dealkylation to form a phenolic metabolite (LAP-OH), *N*-hydroxylation to form a secondary hydroxylamine (*N*-OH-LAP), and *N*-dealkylation giving rise to a primary amine (*N*-dealkyl-LAP). The time course for metabolite formation differed markedly between CYP3A4 and CYP3A5 (Fig. 4, C and D). In CYP3A4 incubations, each metabolite was formed rapidly and in a linear manner during the early phase of the incubation (0.5–2 minutes). Product formation plateaued around 10 minutes, with *N*-OH-LAP levels decreasing markedly (Fig. 4C). In CYP3A5 incubations, LAP-OH was the predominant metabolite formed with relative levels increasing linearly up to 10 minutes. After 30 minutes of incubation, the levels of LAP-OH formed by CYP3A5 were approximately 2-fold higher than levels by CYP3A4 (Fig. 4D).

Relative Contribution of P450 Enzymes to Lapatinib Metabolism. To further evaluate which P450 enzymes contribute to the metabolism of lapatinib, the drug was incubated with a panel of individual cDNA-expressed P450 enzymes. Two incubation times, 2 minutes and 20 minutes, were selected to capture differences in metabolite profile with time. CYP3A4 and CYP3A5 were essentially the only P450 enzymes to form the primary oxidative metabolites of lapatinib (LAP-OH, *N*-OH-LAP, and *N*-dealkyl-LAP) (Fig. 5, A and B); however, CYP3A4 and CYP3A5 displayed striking differences in the relative profile of metabolites generated (Fig. 5, A and B). At 2 minutes,

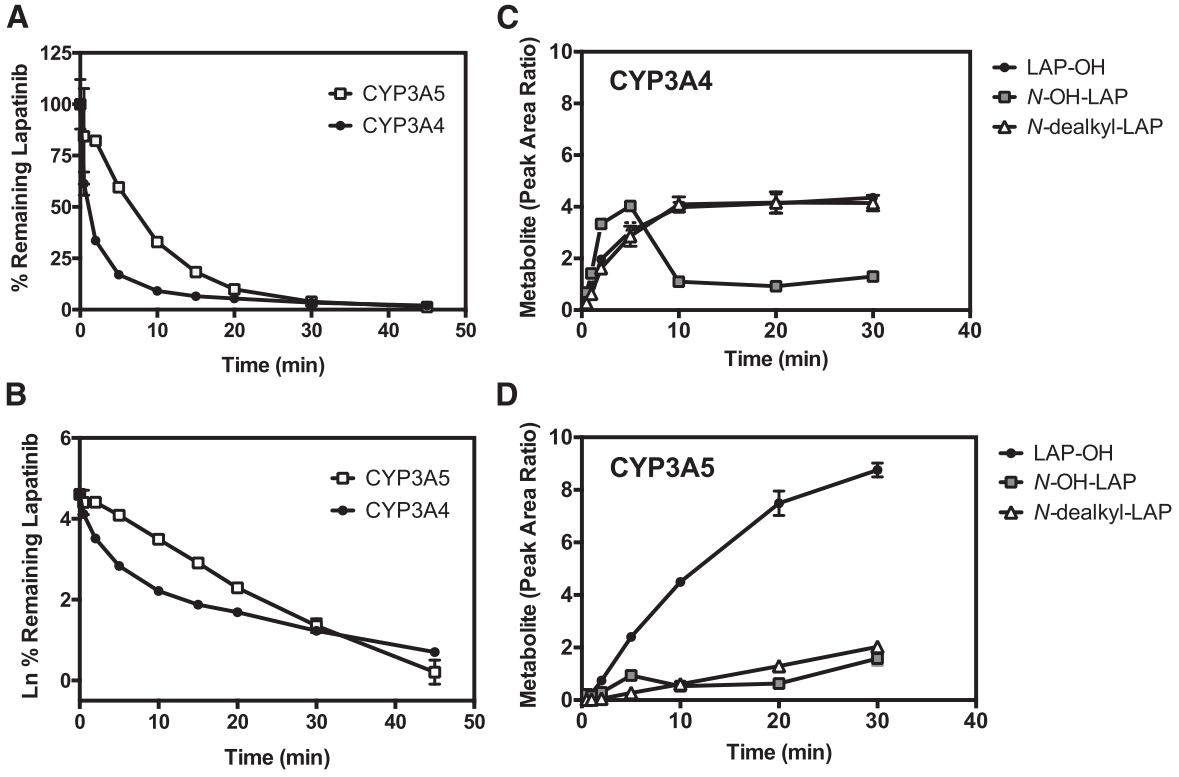

Fig. 4. Lapatinib depletion and metabolite formation by CYP3A4 and CYP3A5. (A and B) Lapatinib (1 μM) was incubated with cDNA-expressed human recombinant CYP3A4 or CYP3A5 (20 nM) with the NADPH-regenerating system over time (1–45 minutes). Samples were analyzed by LC-MS/MS (method B) to determine the percentage of remaining lapatinib. (A) Percent remaining lapatinib and (B) natural log (ln) transformation of percent remaining lapatinib. Data shown were obtained from a single experiment conducted in triplicate. Each data point indicates the mean ± S.D. ($n = 3$). (C and D) Lapatinib (5 μM) was incubated with (C) CYP3A4 and (D) CYP3A5 (20 nM) over time (0.5–30 minutes) to determine the rates of metabolite formation. Relative levels of metabolite were determined using LC-MS/MS analysis (method A). The peak area ratio (metabolite/internal standard) for each metabolite is presented. Data were obtained from a single experiment conducted in triplicate, except at 30 minutes, which was in duplicate. Each data point indicates the mean ± S.D. ($n = 2$ or 3).

CYP3A4 formed the *O*-dealkylated, *N*-hydroxylated, and *N*-dealkylated products of lapatinib to a similar extent, whereas CYP3A5 showed selectivity for the *O*-dealkylation pathway. Markedly higher levels (12-fold) of *N*-OH-LAP and *N*-dealkyl-LAP were formed by CYP3A4 compared with CYP3A5 (Fig. 5A). During the 20-minute incubation with lapatinib, the product ratios for LAP-OH, *N*-OH-LAP, and *N*-dealkyl-LAP formation by CYP3A5/CYP3A4 were 1.25, 0.29, and 0.30, respectively (Fig. 5B).

GSH Trapping Studies with Individual P450 Enzymes. The bioactivation of lapatinib to form the reactive quinoneimine metabolite occurs via two steps: 1) *O*-dealkylation of lapatinib forms the phenolic metabolite (LAP-OH), which contains a *p*-hydroxyaniline moiety; and 2) further oxidation generates the electrophilic quinoneimine product (Teng et al., 2010). GSH adducts of the putative quinoneimine were previously identified in GSH trapping studies from the incubation of lapatinib or *O*-dealkylated lapatinib with HLMs and recombinant CYP3A enzymes (Teng et al., 2010; Chan et al., 2012). To determine the relative contribution of individual P450 enzymes to the formation of the reactive quinoneimine, GSH trapping studies were performed with a panel of cDNA-expressed P450 enzymes using both lapatinib and LAP-OH as substrates. The results of this analysis confirm previous findings that both CYP3A4 and CYP3A5 can form reactive metabolite-GSH adducts from lapatinib or LAP-OH (Fig. 5, C and D). Interestingly, CYP2D6 also contributed to GSH adduct formation from LAP-OH but not from lapatinib (Fig. 5D).

Kinetic Analysis of Lapatinib *O*-Dealkylation and Reactive Metabolite-GSH Adduct Formation by CYP3A4 and CYP3A5. Whereas previous studies have shown that both CYP3A4 and CYP3A5 are capable of lapatinib bioactivation to form the reactive quinoneimine (Teng et al., 2010; Chan et al., 2012), the relative contribution of each enzyme has not been quantitatively determined. Thus, to provide a quantitative assessment of the roles of CYP3A4 and CYP3A5 in lapatinib bioactivation, the kinetic parameters of lapatinib *O*-dealkylation and quinoneimine-GSH adduct formation were examined using CYP3A4 and CYP3A5 supersomes. For LAP-OH formation, a short (2-minute) incubation period was used to ensure the linearity of product formation with respect to time and enzyme concentration. Kinetic parameters apparent K_m and k_{cat} for LAP-OH formation were estimated using two different lots of each of recombinant CYP3A4 and CYP3A5. The mean apparent K_m and k_{cat} values for CYP3A4 were 2.7 ± 0.96 μM and 16 ± 0.74 min^{-1}, respectively, and the mean K_m and k_{cat} for CYP3A5 were 1.7 ± 0.60 μM and 1.9 ± 0.15 min^{-1} (mean ± S.E.M., $n = 2$ lots for each enzyme, from two independent experiments), respectively. Differences in the mean apparent K_m values for were not statistically significant ($P = 0.5040$, $n = 2$, unpaired two-tailed *t* test); however, the mean k_{cat} values indicate that CYP3A4 turned over lapatinib more rapidly compared with CYP3A5 ($P = 0.0029$, $n = 2$). Overall, CYP3A4 displayed a 5.2-fold higher catalytic efficiency (CYP3A4 k_{cat}/K_m = 6.8 ± 2.2 μM^{-1} min^{-1}, mean ± S.E.M., $n = 2$) compared with CYP3A5 (CYP3A5

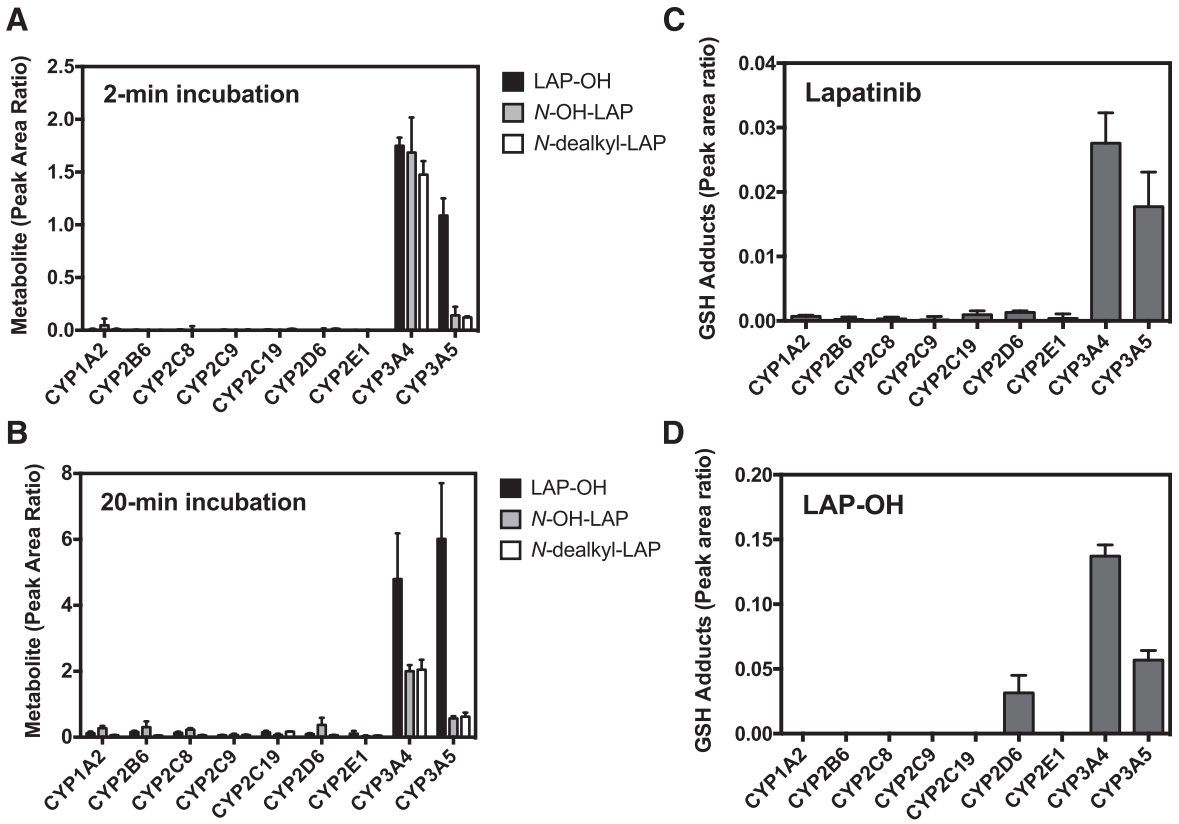

Fig. 5. Relative contribution of P450 enzymes to lapatinib metabolism. (A) Lapatinib (5 μM) was incubated with each of a panel of human recombinant P450 enzymes (20 nM) for 2 minutes or (B and C) for 20 minutes supplemented with 5 mM GSH. (A) Formation of primary lapatinib metabolites (2-minute incubation) was determined using LC-MS/MS analysis (method A). (B) Formation of primary lapatinib metabolites and (C) reactive metabolite-GSH adducts from lapatinib (20-minute incubation) were determined using LC-MS/MS analysis (method C). (D) LAP-OH (5 μM) was incubated with each of a panel of human recombinant P450 enzymes (20 nM) supplemented with 5 mM GSH for 20 minutes. Formation of reactive metabolite-GSH adducts from LAP-OH was determined using LC-MS/MS analysis (method A). The peak area ratio (metabolite/internal standard) for each metabolite is presented. For each graph, data were obtained from a single experiment conducted in triplicate. Bars indicate the mean ± S.D. ($n = 3$).

$k_{cat}/K_m = 1.3 \pm 0.53\ \mu M^{-1}\ min^{-1}$, mean ± S.E.M., $n = 2$) ($P = 0.1327$, unpaired two-tailed t test) (Fig. 6A).

To evaluate interday variability in LC-MS/MS analysis of kinetic assays, the formation of LAP-OH by CYP3A5 supersomes (lot 5258001) from a single experiment conducted in triplicate on 1 day was analyzed by LC-MS/MS (single injection of each triplicate sample) on two separate days. The kinetic parameters, apparent K_m and k_{cat}, from day 1 of LC-MS/MS analysis were 1.0 ± 0.54 μM and 2.0 ± 0.22 min^{-1}, respectively, and the apparent K_m and k_{cat} from day 2 of LC-MS/MS analysis were 1.5 ± 0.81 μM and 2.2 ± 0.26 min^{-1}, respectively. Comparison of the nonlinear regression fit to the Michaelis-Menten model for each data set using the extra sum-of-squares F test in GraphPad Prism 6 software indicated that the differences in apparent K_m and k_{cat} values were not statistically significant (comparison of apparent K_m values, $P = 0.5950$, $F = 0.2860$; comparison of k_{cat}, $P = 0.7235$, $F = 0.1264$). The mean K_m and k_{cat} for CYP3A5 lot 52580001 from the 2 days of LC-MS/MS analysis were 1.2 ± 0.23 μM and 2.1 ± 0.058 min^{-1} (mean ± S.E.M.).

For quinoneimine-GSH adduct formation, a 20-minute incubation period was used because product formation was found to be linear over this time period (data not shown). The kinetic parameters, apparent K_m and k_{cat} (maximum relative GSH adduct levels), were estimated by GSH adduct peak area/d_4-LAP-OH internal standard peak area to obtain the peak area ratio. Preliminary kinetic data from CYP3A4 and CYP3A5 supersomes suggested that CYP3A5 was more efficient at forming quinoneimine-GSH adducts from lapatinib compared with CYP3A4 (data not shown). When this analysis was repeated with three different lots each of CYP3A4 and CYP3A5 supersomes, the relative k_{cat} (peak area ratio) values for CYP3A5 were markedly lower compared with preliminary studies. The data shown in Figs. 6B are the mean values from three different lots each of CYP3A4 and CYP3A5 supersomes (independent experiments were conducted with each lot of enzyme in duplicate or triplicate). For the three newer enzyme lots, the mean apparent K_m values for GSH adduct formation by CYP3A4 and CYP3A5 supersomes were 6.0 ± 0.77 μM and 4.1 ± 0.82 μM (mean ± S.E.M., $n = 3$), respectively. Differences in the apparent K_m values for CYP3A4 and CYP3A5 were not statistically significant ($P = 0.1646$, $n = 3$, unpaired two-tailed t test). The mean k_{cat} (peak area ratio) for CYP3A4 (0.048 ± 0.010, mean ± S.E.M., $n = 3$) was significantly higher compared with the mean k_{cat} for CYP3A5 (0.0075 ± 0.0012, mean ± S.E.M., $n = 3$) ($P = 0.0160$, unpaired two-tailed t test). Using the mean values for these parameters indicated that CYP3A4 was the more efficient bioactivating enzyme by a factor of 4-fold as measured by k_{cat}/K_m (CYP3A4 = 0.0082 ± 0.0018 vs. CYP3A5 = 0.0021 ± 0.00065, mean ± S.E.M., $n = 3$) ($P = 0.0316$, unpaired two-tailed t test) (Fig. 6B).

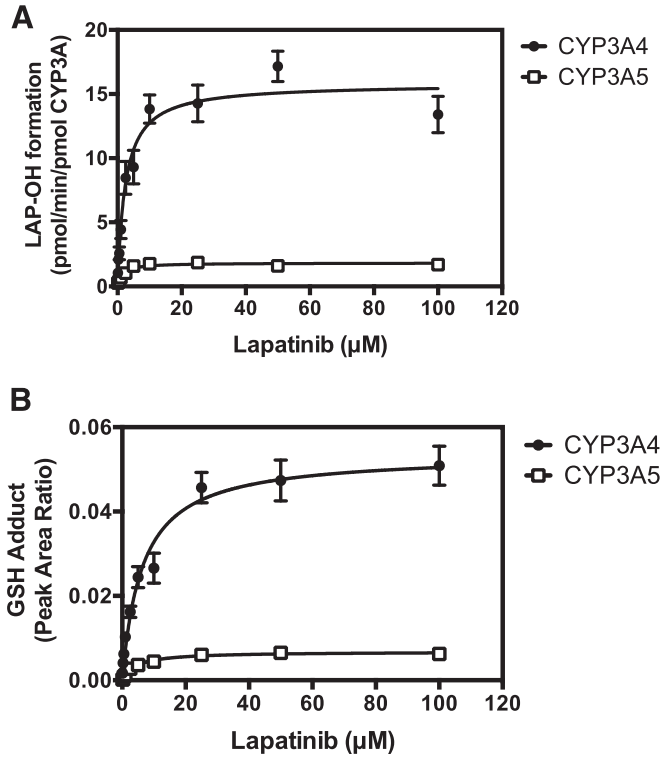

Fig. 6. Kinetics of lapatinib *O*-dealkylation and reactive metabolite-GSH adduct formation by CYP3A4 and CYP3A5. (A) Lapatinib (0.1-100 μM) was incubated with two different lots each of human recombinant CYP3A4 and CYP3A5 (20 nM) supplemented with an NADPH-regenerating system for 2 minutes. Formation of *O*-dealkylated lapatinib (LAP-OH) was measured by LC-MS/MS (Method C). LAP-OH was quantified using an authentic chemical standard. Two independent experiments were conducted in triplicate with two lots each of CYP3A4 and CYP3A5 supersomes. Data points indicate the mean ± S.E.M. ($n = 6$). (B) Lapatinib (0.1–100 μM) was incubated with three different lots each of human recombinant CYP3A4 and CYP3A5 (20 nM) supplemented with 5 mM GSH and an NADPH-regenerating system for 20 minutes. Relative levels of reactive metabolite-GSH adducts were measured by LC-MS/MS (method C). The GSH adduct peak area ratio (GSH adduct/d_4-LAP-OH internal standard) is shown. Data shown are from four independent experiments conducted in duplicate or triplicate with three lots each of CYP3A4 and CYP3A5 supersomes. Data points indicate the mean ± S.E.M. ($n = 11$).

To evaluate interday variability in kinetic assays for GSH adduct formation, independent experiments with CYP3A4 lot 5322004 and CYP3A5 lot 5350002 conducted in triplicate were repeated and analyzed by LC-MS/MS on separate days for comparison. The apparent K_m and k_{cat} (peak area ratio) values for CYP3A4 lot 5322004 from experiment day 1 were 7.6 ± 2.2 μM and 0.065 ± 0.0053 (LC-MS/MS analysis of the same samples was repeated on two separate days), and the apparent K_m and k_{cat} (peak area ratio) values from experiment day 2 were 7.2 ± 1.6 μM and 0.058 ± 0.0036 (LC-MS/MS analysis on a single day). The mean estimated apparent K_m and k_{cat} values for CYP3A4 lot 5322004 from the two independent experiments were 7.5 ± 1.4 μM and 0.062 ± 0.0032 (n = two independent experiments), respectively. Comparison of the data sets obtained from experiment days 1 and 2 using nonlinear regression fit to the Michaelis-Menten model and analyzed with the extra sum-of-squares F test in GraphPad Prism 6 software indicated that the differences in apparent K_m and k_{cat} values were not statistically significant (apparent K_m values 7.6 ± 2.2 μM vs. 7.2 ± 1.6 μM, $P = 0.8705$, $F = 0.02680$; and k_{cat} values 0.065 ± 0.0053 vs. 0.058 ± 0.0036, $P = 0.3024$, $F = 1.083$). The estimated k_{cat}/K_m values (0.0085 vs. 0.0081) from the repeated experiments were also similar.

For CYP3A5 lot 5350002, three independent experiments were conducted on separate days to assess day-to-day variation. The apparent K_m and k_{cat} (peak area ratio) values for GSH adduct formation by CYP3A5 lot 5350002 from experiment day 1 were 3.9 ± 1.9 μM and 0.0050 ± 0.00061, respectively; however, when the experiment was repeated on a second day, the estimated apparent K_m and k_{cat} (peak area ratio) were 20.0 ± 5.5 μM and 0.010 ± 0.0010, respectively. This large difference in apparent K_m suggested an experimental error, and the experiment was repeated a third time. The apparent K_m and k_{cat} values from experiment day 3 were 7.1 ± 1.4 μM and 0.0055 ± 0.00030, respectively. Analysis of the apparent K_m values (2.5 ± 0.60, 5.0 ± 1.2, 2.9 ± 1.7, 20.0 ± 5.5, and 7.1 ± 1.4 μM) from the five total experiments with CYP3A5 supersomes using Grubbs' test to detect outliers with GraphPad Prism 6 software indicated that the high apparent K_m (20 μM) from experiment day 2 with CYP3A5 lot 5350002 was an outlier compared with the data from other experiments. This wide variation may be due to experimental error in the assay. Thus, data from experiment

day 2 with CYP3A5 lot 5350002 were excluded from the calculation of mean apparent K_m and k_{cat} parameters for GSH adduct formation by CYP3A5. Comparison of the data obtained from CYP3A5 lot 5350002 experiment days 1 and 3 using nonlinear regression fit to the Michaelis-Menten model and analyzed with the extra sum-of-squares F test in GraphPad Prism 6 software indicated that the differences in apparent K_m and k_{cat} values were not statistically significant (apparent K_m values 3.9 ± 1.9 μM vs. 7.1 ± 1.4 μM, $P = 0.2628$, $F = 1.279$; and k_{cat} values 0.0050 ± 0.00061 vs. 0.0055 ± 0.00030, $P = 0.5008$, $F = 0.4592$). The mean estimated apparent K_m and k_{cat} values from experiment days 1 and 3 with CYP3A5 lot 5350002 were 5.5 ± 1.6 μM and 0.0052 ± 0.00025 ($n = 2$ independent experiments), respectively.

To evaluate intraday variability in LC-MS/MS analysis, samples from a single experiment (CYP3A5 lot 5350002) conducted in triplicate ($n = 3$) on one day were analyzed by two repeat injections on the LC-MS/MS system on the same day. The apparent K_m and k_{cat} (peak area ratio) from LC-MS/MS sequence 1 were 6.9 ± 1.7 μM and 0.0060 ± 0.00040, respectively, and the apparent K_m and k_{cat} values from sequence 2 were 7.3 ± 1.7 μM and 0.0050 ± 0.00032, respectively. The mean apparent K_m and k_{cat} values from the two injections were 7.1 ± 1.4 μM and 0.0055 ± 0.00028. Comparison of the data sets obtained from LC-MS/MS injections 1 and 2 using nonlinear regression fit with the extra sum-of-squares F test in GraphPad Prism software indicated that the differences in apparent K_m and k_{cat} values were not statistically significant (apparent K_m values 6.9 ± 1.7 μM vs. 7.3 ± 1.7 μM, $P = 0.8706$, $F = 0.02676$; and k_{cat} values 0.0060 ± 0.00040 vs. 0.0050 ± 0.00032, $P = 0.0607$, $F = 3.664$). In addition, the internal standard (d_4-LAP-OH) peak areas were compared between each set of triplicate samples from two separate experiments examining the kinetics of GSH adduct formation by CYP3A4 and CYP3A5 supersomes. The experimental samples in this analysis were analyzed by LC-MS/MS on the same day. No remarkable difference was seen in the internal standard peak areas between each set of triplicate samples (single injection for each sample) run sequentially within a single experiment. The mean internal standard peak areas between the two separate experiments analyzed on the same day were compared using an unpaired two-tailed t test, and the mean values were not statistically different ($P = 0.5436$).

During the course of the study, differences in the kinetic parameters for GSH adduct formation were observed between the different lots of CYP3A4 and CYP3A5 supersomes. Comparison of mean estimated apparent K_m values from nonlinear regression fit was performed by extra sum-of-squares F test, and the results indicated that differences in mean apparent K_m values between enzyme lots were not statistically significant: mean apparent K_m values for CYP3A4 lots (3288855, 5224002, and 5322004) were 5.6 ± 1.3, 4.9 ± 0.91, and 7.5 ± 2.2 μM ($P = 0.3442$, $F = 1.077$); mean apparent K_m values for CYP3A5 lots (4191001, 5258001, 5350002) were 2.5 ± 0.60, 5.0 ± 1.2, and 4.8 ± 1.2 μM ($P = 0.1197$, $F = 2.167$); however, the estimated k_{cat} (peak area ratio) values between different enzyme lots differed significantly. The mean k_{cat} (peak area ratio) values for CYP3A4 lots were 0.055 ± 0.0026, 0.029 ± 0.0018, and 0.062 ± 0.0053 ($P = 0.0005$, $F = 8.288$); mean k_{cat} (peak area ratio) values for CYP3A5 lots were 0.0080 ± 0.00045, 0.0092 ± 0.00059, and 0.0051 ± 0.00061 ($P < 0.0001$, $F = 22.03$). A correlation analysis was performed to examine whether differences in the kinetic parameters between CYP3A4 and CYP3A5 enzyme lots were correlated with the reported enzyme activity. For CYP3A4 lots (3288855, 5224002, 5322004), the testosterone 6β-hydroxylase activities were 170, 180, and 150 pmol product/(min × pmol P450), respectively, and the mean relative kinetic parameters for GSH adduct formation (k_{cat}/K_m) were 0.0052, 0.011, and 0.0083, respectively. For CYP3A5 lots (4191001, 5258001, 5350002), the testosterone 6β-hydroxylase activities were 68, 49, 22 pmol product/(min × pmol P450), respectively, and the mean relative kinetic parameters for GSH adduct formation (k_{cat}/K_m) were 0.0032, 0.0018, and 0.0011, respectively. Overall, the enzyme activity was positively correlated with GSH adduct formation ($r = 0.89$; $R^2 = 0.79$; $P = 0.0174$, $n = 6$).

Incubation of CYP3A4 with higher concentrations of lapatinib for 20 minutes could be expected to cause substrate inhibition. To test this, the pooled data obtained from substrate saturation assays with CYP3A4 and CYP3A5 supersomes (three different lots for each enzyme) were evaluated for curve fit to the Michaelis-Menten model compared with the substrate inhibition model using nonlinear regression (GraphPad Prism 6). Data from one out of three of the CYP3A4 lots (lot 5224002) and one out of three of the CYP3A5 lots (lot 5350002) fit to the substrate inhibition model; however, the Michaelis-Menten equation was determined to be the preferred model for both sets of data ($P = 0.5616$, $F = 0.3455$ for CYP3A4 lot 5224002, and $P = 0.2141$, $F = 1.579$ for CYP3A5 lot 5350002). Data from the remaining lots of CYP3A4 and CYP3A5 supersomes did not fit to the substrate inhibition model, and the Michaelis-Menten equation was the preferred model. Thus, an apparent substrate inhibition was not readily observed for GSH adduct formation based on the kinetic analysis in this study.

Effect of Chemical Inhibitors on Metabolite Formation. To verify the results from recombinant P450 enzymes, metabolism studies were carried out with pooled HLMs in the presence of selective P450 chemical inhibitors. First, lapatinib was incubated with HLMs in the presence of chemical inhibitors for CYP1A2, CYP2B6/CYP2C19, CYP2C9, CYP2D6, CYP2E1, and CYP3A4/5. Ketoconazole, a potent inhibitor of CYP3A4/5, decreased the formation of lapatinib primary metabolites LAP-OH, *N*-OH-LAP, and *N*-dealkyl-LAP by 79% ± 15% (mean ± S.D., $n = 3$) ($P = 0.0071$), 61% ± 8% ($P = 0.0015$), 90% ± 10% ($P = 0.0010$), respectively (Fig. 7A).

GSH trapping studies were also performed to determine the effect of P450 inhibitors on the formation of reactive quinoneimine-GSH adducts using both lapatinib and LAP-OH as substrates. As shown in Fig. 7B, ketoconazole decreased the levels of quinoneimine-GSH adducts formed from lapatinib by 89% ± 19% (mean ± S.D., $n = 3$) ($P = 0.0096$) compared with vehicle control. In incubations with LAP-OH, ketoconazole reduced the levels of quinoneimine-GSH adducts by 60% ± 8% (mean ± S.D., $n = 6$) ($P < 0.0001$) compared with vehicle (Fig. 7C). Sulfaphenazole also decreased the formation of GSH adducts by 45% ± 9% (mean ± S.D., $n = 6$) ($P = 0.0006$) compared with control. Coincubation with α-naphthoflavone increased the levels of quinoneimine-GSH adducts to 146% ± 7% (mean ± S.D., $n = 6$) ($P = 0.0005$) of control levels. Although α-naphthoflavone is a known CYP1A2 inhibitor, these data suggest a possible activation effect on CYP3A4-mediated LAP-OH metabolism (Shou et al., 1994). Activation of lapatinib metabolism by α-naphthoflavone has not been reported previously. Only coincubation of α-naphthoflavone with LAP-OH, and not lapatinib, led to a statistically significant increase in generation-reactive metabolite-GSH adducts compared with vehicle control (Fig. 7C). Coincubation with other inhibitors did not result in a statistically significant increase in metabolite formation. Although CYP2D6 was shown to form quinoneimine-GSH adducts from LAP-OH in the recombinant P450 enzyme screen (Fig. 5D), the CYP2D6 inhibitor quinidine did not alter the formation of GSH adducts.

Effect of CYP3A4-Selective Inhibitors on Metabolite Formation. In a separate series of experiments, the CYP3A4-selective inhibitors SR-9186 and CYP3cide were used to distinguish the contribution of CYP3A4 versus CYP3A5 to the formation of reactive metabolite-GSH adducts from lapatinib. SR-9186 is a competitive CYP3A4 inhibitor (Li et al., 2012), and CYP3cide is a time-dependent mechanism-based CYP3A4 inactivator (Walsky et al., 2012). Ketoconazole was used as a

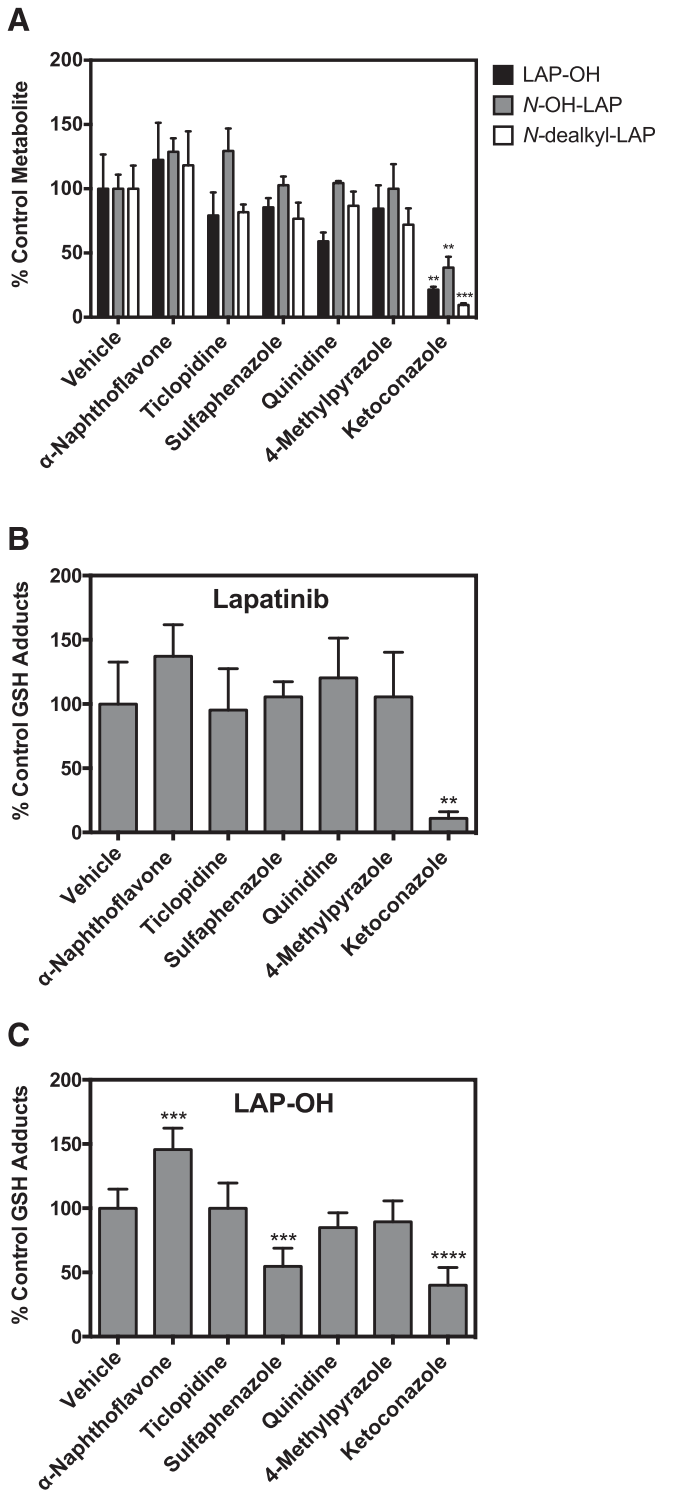

Fig. 7. Effect of P450 chemical inhibitors on lapatinib metabolite formation. (A and B) Lapatinib (5 μM) was incubated with pooled HLMs (0.1 mg/ml) supplemented with 5 mM GSH in the presence or absence of P450 selective chemical inhibitors for 20 minute.s (See *Materials and Methods* for details regarding P450 inhibitors). (A and B) Data were obtained from a single experiment conducted in triplicate. Bars indicate the mean ± S.D. (n = 3). (C) LAP-OH (5 μM) was incubated with pooled HLMs (0.1 mg/ml) supplemented with 5 mM GSH in the presence or absence of P450-selective chemical inhibitors for 20 minutes. Relative metabolite formation was measured by LC-MS/MS (method C). The percent control metabolite or GSH adduct formation was calculated relative to vehicle control incubations with no inhibitor. (C) Data were compiled from two independent experiments, each conducted in triplicate. Bars indicate the mean ± S.D. (n = 6). Comparisons of inhibitor versus control were performed using an unpaired two-tailed t test. $^{**}P < 0.01$; $^{***}P \leq 0.001$; $^{****}P < 0.0001$.

pan-CYP3A inhibitor to estimate the baseline CYP3A contribution. SR-9186 reduced the formation of GSH adducts by 78% ± 4% (n = 3, $P < 0.0001$), and CYP3cide decreased GSH adducts formation by 72% ± 8% (n = 6, P = 0.0004) compared with control (Fig. 8, A and B). Ketoconazole resulted in >90% inhibition under both experimental conditions. The difference between inhibition by SR-9186 and ketoconazole was 16% ± 3% (n = 3, P = 0.0038), and the difference between inhibition by CYP3cide and ketoconazole was 22% ± 8% (n = 6, P = 0.0213), indicative of residual CYP3A5 activity under conditions chosen to mimic physiologic concentrations of the drug.

Discussion

Lapatinib has two known pathways of bioactivation, which may contribute to enzyme inactivation, drug-drug interactions, or drug-induced liver injury (Teng et al., 2010; Takakusa et al., 2011). One pathway is via *N*-hydroxylation and *N*-dealkylation of the secondary amine to form a reactive nitroso intermediate (Takakusa et al., 2011). Previous reports indicate that the nitroso intermediate forms a metabolic intermediate complex with the P450 heme iron resulting in quasi-irreversible inactivation of CYP3A4 (Takakusa et al., 2011; Barbara et al., 2013). The second bioactivation pathway is via lapatinib *O*-dealkylation and further oxidation to form of a reactive quinoneimine (Teng et al., 2010). This latter pathway is thought to result in irreversible inactivation of CYP3A5 and initiate lapatinib immune-mediated hepatotoxicity through covalent modification of cellular proteins (Chan et al., 2012). Understanding the relative roles of CYP3A4 and CYP3A5 in lapatinib bioactivation is relevant because *CYP3A5* is highly polymorphic, and *CYP3A5* genetic variation may influence interindividual variability in the generation of reactive metabolites of lapatinib. This is the first report to use reaction phenotyping approaches and kinetic (K_m, k_{cat}) analyses to provide a quantitative assessment of the CYP3A4 versus CYP3A5 enzymatic contributions to lapatinib metabolism and the formation of reactive quinoneimine-GSH adducts.

Substrate depletion experiments showed that CYP3A4 was more efficient than CYP3A5 in the overall metabolism of lapatinib; however, the decreased rate of metabolism by CYP3A4 over time suggests time-dependent inhibition of the enzyme. Both CYP3A4 and CYP3A5 have previously been shown to undergo mechanism-based inactivation by lapatinib in vitro; however, the kinetics of inactivation differ significantly between each enzyme (Teng et al., 2010; Chan et al., 2012). The reported k_{inact} and K_I values for CYP3A4 by lapatinib were 0.020 min^{-1} and 1.71 μM (Teng et al., 2010), and the k_{inact} and K_I values for CYP3A5 were 0.023 min^{-1} and 37.6 μM (Chan et al., 2012). Thus, the estimated k_{inact}/K_I ratio is nearly 20-fold higher for CYP3A4 compared with CYP3A5, indicating that lapatinib inactivates CYP3A4 to a greater extent than CYP3A5. Other CYP3A substrates, such as dronedarone (Hong et al., 2016), have also been shown to display differences in inactivation characteristics for CYP3A4 and CYP3A5. Time-dependent inhibition of CYP3A4 by lapatinib may be clinically relevant based on previous studies regarding the pharmacokinetics of lapatinib in vivo. An increase in lapatinib serum concentrations and $t_{1/2}$ over time was reported with multiple dosing, suggesting time-dependent autoinhibition of lapatinib clearance (Burris et al., 2005).

Previous in silico docking and metabolic profiling studies suggested that lapatinib *N*-dealkylation and *N*-hydroxylation are predominately catalyzed by CYP3A4, whereas CYP3A5 may preferentially catalyze the *O*-dealkylation pathway (Takakusa et al., 2011; Chan et al., 2012; Barbara et al., 2013). The results of the present study are consistent with these findings. Both recombinant CYP3A4 and CYP3A5 generated each of the primary metabolites of lapatinib through *N*-dealkylation, *N*-hydroxylation, and *O*-dealkylation; however, the time course and

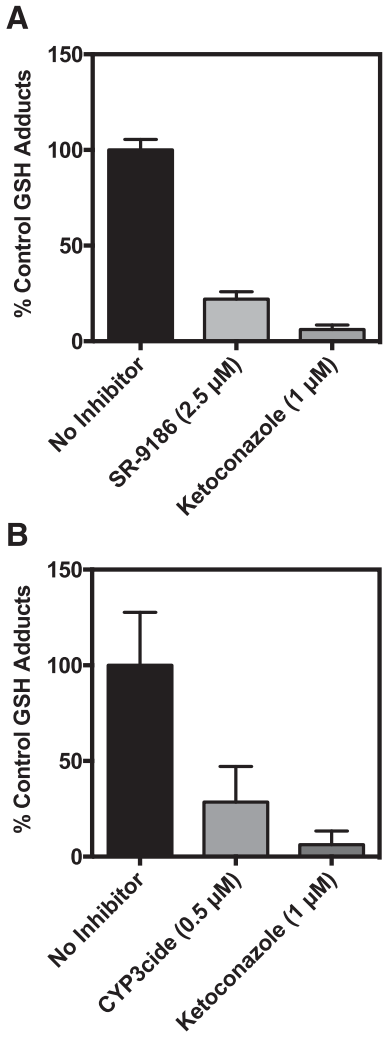

Fig. 8. Effect of CYP3A-selective inhibitors on GSH adduct formation. Lapatinib (5 μM) was incubated with pooled HLMs (0.1 mg/ml) with or without CYP3A inhibitors in the presence of 5 mM GSH and an NADPH-regenerating system for 20 minutes. (A) SR-9186 (2.5 μM) is a competitive CYP3A4 inhibitor. Data were obtained from a single experiment conducted in triplicate. Bars indicate the mean ± S.D. (n = 3). (B) CYP3cide (0.5 μM) is a time-dependent CYP3A4 inactivator (5 minutes preincubation). Ketoconazole (1 μM) was used as a competitive pan-CYP3A inhibitor. Relative levels of reactive metabolite-GSH adducts were measured by LC-MS/MS (method C). The percent control GSH adduct formation was calculated relative to vehicle control incubations with no inhibitor. Data were compiled from the two independent experiments; each experiment was conducted in triplicate. Bars indicate the mean ± S.D. (n = 6).

extent of metabolite generation differed by enzyme. Similar to previous reports, *N*-dealkylated and *N*-hydroxylated metabolites were higher by CYP3A4 compared with CYP3A5. The marked decline in the levels of *N*-OH-LAP during longer incubation times with CYP3A4 may be because *N*-OH-LAP can be further oxidized to a nitroso intermediate (Takakusa et al., 2011; Barbara et al., 2013). On the other hand, formation of LAP-OH was higher in incubations with CYP3A5 compared with CYP3A4 during longer incubations. One of the differences between the present and previous studies is that metabolic incubations in this study were conducted at therapeutic concentrations of lapatinib (1—5 μM) to mimic physiologic conditions compared with previous studies which used higher concentrations (50 μM) of the drug (Teng et al., 2010; Takakusa et al., 2011; Chan et al., 2012; Barbara et al., 2013). In addition, attention was given to the time course of metabolite generation to ensure linearity of product formation.

Teng et al. (2010) and Chan et al. (2012) reported qualitative evidence for CYP3A4/5-mediated formation of quinoneimine-GSH adducts from lapatinib. The present study provides quantitative insight into the relative roles of CYP3A4 and CYP3A5 in lapatinib bioactivation by examining the kinetics of lapatinib *O*-dealkylation and quinoneimine-GSH adduct formation. Using the mean k_{cat}/K_m values obtained from kinetic analysis of two to three separate lots each of cDNA-expressed CYP3A4 and CYP3A5 indicated that CYP3A4 was 4- to 5-fold more efficient than CYP3A5 at lapatinib *O*-dealkylation and quinoneimine-GSH adduct formation. Variations in the kinetic parameters estimated between different lots of enzyme could be due to interday variability in kinetic assays as well as lot-to-lot differences in enzyme activity between batches of CYP3A4 and CYP3A5 supersomes. Correlation analysis indicated a positive correlation between testosterone 6β-hydroxylase activity for the different lots of CYP3A supersomes and GSH adduct formation, although the sample number was small (n = 6 lots). It was noted that the reported testosterone 6β-hydroxylase activity was lower overall for CYP3A5 compared with CYP3A4, which is consistent with previous studies (Patki et al., 2003).

Microsomal incubations with P450-selective chemical inhibitors confirmed that CYP3A4 and CYP3A5 are the primary P450s responsible for quinoneimine-GSH adduct formation using lapatinib or LAP-OH as the substrate. The observation that sulfaphenazole also reduced GSH adduct formation from LAP-OH suggests that the involvement of other P450s in lapatinib bioactivation cannot be ruled out. The CYP3A4-selective inhibitors SR-9186 and CYP3cide decreased quinoneimine-GSH adduct formation to a lesser extent (~20% less) than the pan-CYP3A inhibitor ketoconazole. This finding indicates that the remaining CYP3A5 activity in pooled HLMs is likely responsible for generating the reactive quinoneimine-GSH adducts from lapatinib.

To date, no studies have been reported on the relationship between *CYP3A* genotype and the pharmacokinetics or toxicity of lapatinib in vivo. We have previously found that in individual *CYP3A5*-genotyped human liver microsomes, the levels of reactive quinoneimine-GSH adducts generated from LAP-OH were 1.7-fold higher in CYP3A5 expressors (*CYP3A5*1* carriers) versus nonexpressors (*CYP3A5*3/*3* livers) (P = 0.03) (Ho et al., 2015). Chan et al. (2014) also reported 2-fold higher levels of GSH adducts derived from lapatinib in HLMs from *CYP3A5*1/*1* donors compared with *CYP3A5*3/*3* genotyped human liver samples. These data suggest that *CYP3A5* polymorphism may contribute to variations in individual exposure to the reactive, potentially toxic quinoneimine metabolite of lapatinib. Whether the differences in reactive metabolite generation have a clinically significant impact is unknown and will require further investigation.

Previous reports indicate that the systemic exposure of lapatinib is significantly altered by coadministration of the CYP3A inhibitor ketoconazole or the CYP3A4 inducer carbamazepine (Smith et al., 2009). In addition, Teo et al. (2012) demonstrated that concurrent use of lapatinib with dexamethasone (CYP3A4 inducer) in metastatic breast cancer patients increased the risk of lapatinib-induced hepatotoxicity, suggesting the involvement of CYP3A-mediated bioactivation. We have previously shown that LAP-OH was more cytotoxic than lapatinib itself in the HepaRG hepatic cell model (Hardy et al., 2014). CYP3A4 induction by dexamethasone and rifampin potentiated lapatinib-induced cytotoxicity, which was correlated with increased formation of LAP-OH and reactive quinoneimine-cysteine conjugates (Hardy et al., 2014). More recently, Cameron and colleagues showed that *O*-dealkylated lapatinib induced mitochondrial stress and activation of the oxidative stress responsive transcription factor nuclear factor erythroid 2-related factor 2 (Nrf2) in HepG2 cells (Eno et al., 2016). Lapatinib

administration to Nrf2-knockout and control mice led to elevated liver transaminases, which levels returned to baseline after repeat dosing in control mice but continued to rise in Nrf2 knockout mice, indicating that Nrf2 may be involved in cellular defense against lapatinib-induced hepatotoxicity (Eno et al., 2016).

Several mechanisms have been proposed to play a role in the development of lapatinib-induced hepatotoxicity, and it is likely that multiple pathways are involved. One pathway is through lapatinib *O*-dealkylation and subsequent oxidation to the reactive quinoneimine, which may result in covalent protein modification, potentially leading to direct cell stress or activation of immune responses (Park et al., 2005). Evidence for immune-mediated toxicity has been shown through a series of pharmacogenomic investigations, in which the human leukocyte antigen (HLA) allele *HLA-DRB1*07:01* (and *HLA-DQA1*02:01)* was found to be associated with severe hepatotoxicity in a subset of metastatic breast cancer patients treated with lapatinib (Spraggs et al., 2011; Spraggs et al., 2012; Spraggs et al., 2013; Schaid et al., 2014; Parham et al., 2016). Activation of the adaptive immune response triggered by covalent binding of drug and/or reactive metabolites to cellular proteins leading to hapten formation and HLA recognition has been suggested as a potential mechanism (Spraggs et al., 2011). An alternative hypothesis was recently presented to suggest that lapatinib itself may trigger immune activation by enhancing ligand binding to HLA-DRB1*07:01 (Hirasawa et al., 2015). Inhibition of the bile salt export pump by LAP-OH (Castellino et al., 2012) and induction of mitochondrial impairment (Eno et al., 2016) have also been suggested to contribute to liver injury. Additional studies are required to elucidate the actual mechanisms involved.

In summary, we have shown that both CYP3A4 and CYP3A5 are quantitatively important contributors to the bioactivation of lapatinib to form reactive quinoneimine metabolites. Further studies are needed to explore the bioactivation, inactivation, and transport pathways of lapatinib in vivo to identify the factors that may contribute to lapatinib-induced hepatotoxicity in clinical settings.

Acknowledgments

The authors thank Dr. F. Peter Guengerich and his group (Vanderbilt University) for valuable scientific discussions and editing during the manuscript preparation, Dr. W. Scott Akers (Lipscomb University) for helpful scientific discussions, and Dr. Michael Cameron (Scripps Research Institute) for generously providing the CYP3A4-selective inhibitor SR-9186.

Authorship Contributions

Participated in research design: Towles, Clark, Wahlin, Rettie, Jackson.

Conducted experiments: Towles, Clark, and Jackson.

Contributed new reagents or analysis tools: Uttamsingh.

Performed data analysis: Towles, Clark, Jackson.

Wrote or contributed to the writing of the manuscript: Towles, Clark, Uttamsingh, Rettie, Jackson.

References

Aoyama T, Yamano S, Waxman DJ, Lapenson DP, Meyer UA, Fischer V, Tyndale R, Inaba T, Kalow W, Gelboin HV, et al. (1989) Cytochrome P-450 hPCN3, a novel cytochrome P-450 IIIA gene product that is differentially expressed in adult human liver: cDNA and deduced amino acid sequence and distinct specificities of cDNA-expressed hPCN1 and hPCN3 for the metabolism of steroid hormones and cyclosporine. *J Biol Chem* **264**:10388–10395.

Arteaga CL, Sliwkowski MX, Osborne CK, Perez EA, Puglisi F, and Gianni L (2012) Treatment of HER2-positive breast cancer: current status and future perspectives. *Nat Rev Clin Oncol* **9**: 16–32.

Atkins WM (2005) Non-Michaelis-Menten kinetics in cytochrome P450-catalyzed reactions. *Annu Rev Pharmacol Toxicol* **45**:291–310.

Azim HA, Jr, Agbor-Tarh D, Bradbury I, Dinh P, Baselga J, Di Cosimo S, Greger JG, Jr, Smith I, Jackisch C, Kim SB, et al. (2013) Pattern of rash, diarrhea, and hepatic toxicities secondary to lapatinib and their association with age and response to neoadjuvant therapy: analysis from the NeoALTTO trial. *J Clin Oncol* **31**:4504–4511.

Barbara JE, Kazmi F, Parkinson A, and Buckley DB (2013) Metabolism-dependent inhibition of CYP3A4 by lapatinib: evidence for formation of a metabolic intermediate complex with a nitroso/oxime metabolite formed via a nitrone intermediate. *Drug Metab Dispos* **41**:1012–1022.

Burris HA, 3rd, Hurwitz HI, Dees EC, Dowlati A, Blackwell KL, O'Neil B, Marcom PK, Ellis MJ, Overmoyer B, Jones SF, et al. (2005) Phase I safety, pharmacokinetics, and clinical activity study of lapatinib (GW572016), a reversible dual inhibitor of epidermal growth factor receptor tyrosine kinases, in heavily pretreated patients with metastatic carcinomas. *J Clin Oncol* **23**: 5305–5313.

Castellino S, O'Mara M, Koch K, Borts DJ, Bowers GD, and MacLauchlin C (2012) Human metabolism of lapatinib, a dual kinase inhibitor: implications for hepatotoxicity. *Drug Metab Dispos* **40**:139–150.

Chan ECY, New LS, Chua TB, Yap CW, Ho HK, and Nelson SD (2012) Interaction of lapatinib with cytochrome P450 3A5. *Drug Metab Dispos* **40**:1414–1422.

Chan JCY, Choo DYM, and Chan ECY(2014) Impact of CYP3A5 genetic polymorphism on mechanism-based inactivation by lapatinib, in *19th North American ISSX and 29th JSSX Joint Meeting*; 2014 October 19–23; San Francisco, CA. Abstract P287, International Society for the Study of Xenobiotics, Washington, DC.

Eno MR, El-Gendy Bel-D, and Cameron MD (2016) P450 3A-catalyzed O-dealkylation of lapatinib induces mitochondrial stress and activates Nrf2. *Chem Res Toxicol* **29**:784–796.

Geyer CE, Forster J, Lindquist D, Chan S, Romieu CG, Pienkowski T, Jagiello-Gruszfeld A, Crown J, Chan A, Kaufman B, et al. (2006) Lapatinib plus capecitabine for HER2-positive advanced breast cancer. *N Engl J Med* **355**:2733–2743.

Gorski JC, Hall SD, Jones DR, VandenBranden M, and Wrighton SA (1994) Regioselective biotransformation of midazolam by members of the human cytochrome P450 3A (CYP3A) subfamily. *Biochem Pharmacol* **47**:1643–1653.

Guengerich FP (1999) Cytochrome P-450 3A4: regulation and role in drug metabolism. *Annu Rev Pharmacol Toxicol* **39**:1–17.

Guengerich FP and Bartleson CJ (2008) Preparation of microsomal and cytosolic fractions, in *Principles and Methods of Toxicology*, 5th ed. (Hayes AW, ed) pp 1994–1996, CRC Press, Boca Raton, FL.

Hardy KD, Wahlin MD, Papageorgiou I, Unadkat JD, Rettie AE, and Nelson SD (2014) Studies on the role of metabolic activation in tyrosine kinase inhibitor-dependent hepatotoxicity: induction of CYP3A4 enhances the cytotoxicity of lapatinib in HepaRG cells. *Drug Metab Dispos* **42**: 162–171.

Hirasawa M, Hagihara K, Okudaira N, and Izumi T (2015) The possible mechanism of idiosyncratic lapatinib-induced liver injury in patients carrying human leukocyte antigen-*DRB1*07:01*. *PLoS One* **10**:e0130928.

Ho HK, Chan JC, Hardy KD, and Chan EC (2015) Mechanism-based inactivation of CYP450 enzymes: a case study of lapatinib. *Drug Metab Rev* **47**:21–28.

Hong Y, Chia YM, Yeo RH, Venkatesan G, Koh SK, Chai CLL, Zhou L, Kojodjojo P, and Chan EC (2016) Inactivation of human cytochrome P450 3A4 and 3A5 by dronedarone and *N*-desbutyl dronedarone. *Mol Pharmacol* **89**:1–13.

Houston JB and Kenworthy KE (2000) In vitro-in vivo scaling of CYP kinetic data not consistent with the classical Michaelis-Menten model. *Drug Metab Dispos* **28**:246–254.

Hutzler JM and Tracy TS (2002) Atypical kinetic profiles in drug metabolism reactions. *Drug Metab Dispos* **30**:355–362.

Johnston S, Pippen J, Jr, Pivot X, Lichinitser M, Sadeghi S, Dieras V, Gomez HL, Romieu G, Manikhas A, Kennedy MJ, et al. (2009) Lapatinib combined with letrozole versus letrozole and placebo as first-line therapy for postmenopausal hormone receptor-positive metastatic breast cancer. *J Clin Oncol* **27**:5538–5546.

Kolars JC, Lown KS, Schmiedlin-Ren P, Ghosh M, Fang C, Wrighton SA, Merion RM, and Watkins PB (1994) CYP3A gene expression in human gut epithelium. *Pharmacogenetics* **4**: 247–259.

Kopper L (2008) Lapatinib: a sword with two edges. *Pathol Oncol Res* **14**:1–8.

Kuehl P, Zhang J, Lin Y, Lamba J, Assem M, Schuetz J, Watkins PB, Daly A, Wrighton SA, Hall SD, et al. (2001) Sequence diversity in CYP3A promoters and characterization of the genetic basis of polymorphic CYP3A5 expression. *Nat Genet* **27**:383–391.

Lackey KE (2006) Lessons from the drug discovery of lapatinib, a dual ErbB1/2 tyrosine kinase inhibitor. *Curr Top Med Chem* **6**:435–460.

Lamba JK, Lin YS, Schuetz EG, and Thummel KE (2002) Genetic contribution to variable human CYP3A-mediated metabolism. *Adv Drug Deliv Rev* **54**:1271–1294.

Li X, Song X, Kamenecka TM, and Cameron MD (2012) Discovery of a highly selective CYP3A4 inhibitor suitable for reaction phenotyping studies and differentiation of CYP3A4 and CYP3A5. *Drug Metab Dispos* **40**:1803–1809.

Lin YS, Dowling AL, Quigley SD, Farin FM, Zhang J, Lamba J, Schuetz EG, and Thummel KE (2002) Co-regulation of CYP3A4 and CYP3A5 and contribution to hepatic and intestinal midazolam metabolism. *Mol Pharmacol* **62**:162–172.

Moy B, Kirkpatrick P, Kar S, and Goss P (2007) Lapatinib. *Nat Rev Drug Discov* **6**:431–432.

Moy B, Rappold E, and Williams L (2009) Hepatobiliary abnormalities in patients with metastatic cancer treated with lapatinib (Abstract 1043). *J Clin Oncol* 27 (Suppl 15S).

Parham LR, Briley LP, Li L, Shen J, Newcombe PJ, King KS, Slater AJ, Dilthey A, Iqbal Z, McVean G, et al. (2016) Comprehensive genome-wide evaluation of lapatinib-induced liver injury yields a single genetic signal centered on known risk allele *HLA-DRB1*07:01*. *Pharmacogenomics J* **16**:180–185.

Park BK, Kitteringham NR, Maggs JL, Pirmohamed M, and Williams DP (2005) The role of metabolic activation in drug-induced hepatotoxicity. *Annu Rev Pharmacol Toxicol* **45**:177–202.

Patki KC, Von Moltke LL, and Greenblatt DJ (2003) In vitro metabolism of midazolam, triazolam, nifedipine, and testosterone by human liver microsomes and recombinant cytochromes p450: role of cyp3a4 and cyp3a5. *Drug Metab Dispos* **31**:938–944.

Ramírez J, Innocenti F, Schuetz EG, Flockhart DA, Relling MV, Santucci R, and Ratain MJ (2004) CYP2B6, CYP3A4, and CYP2C19 are responsible for the in vitro N-demethylation of meperidine in human liver microsomes. *Drug Metab Dispos* **32**:930–936.

Rusnak DW, Affleck K, Cockerill SG, Stubberfield C, Harris R, Page M, Smith KJ, Guntrip SB, Carter MC, Shaw RJ, et al. (2001) The characterization of novel, dual ErbB-2/EGFR, tyrosine kinase inhibitors: potential therapy for cancer. *Cancer Res* **61**:7196–7203.

Schaid DJ, Spraggs CF, McDonnell SK, Parham LR, Cox CJ, Ejlertsen B, Finkelstein DM, Rappold E, Curran J, Cardon LR, et al. (2014) Prospective validation of HLA-DRB1*07:01 allele carriage as a predictive risk factor for lapatinib-induced liver injury. *J Clin Oncol* **32**: 2296–2303.

Shimada T, Yamazaki H, Mimura M, Inui Y, and Guengerich FP (1994) Interindividual variations in human liver cytochrome P-450 enzymes involved in the oxidation of drugs, carcinogens and

toxic chemicals: studies with liver microsomes of 30 Japanese and 30 Caucasians. *J Pharmacol Exp Ther* **270**:414–423.
Shou M, Grogan J, Mancewicz JA, Krausz KW, Gonzalez FJ, Gelboin HV, and Korzekwa KR (1994) Activation of CYP3A4: evidence for the simultaneous binding of two substrates in a cytochrome P450 active site. *Biochemistry* **33**:6450–6455.
Smith DA, Koch KM, Arya N, Bowen CJ, Herendeen JM, and Beelen A (2009) Effects of ketoconazole and carbamazepine on lapatinib pharmacokinetics in healthy subjects. *Br J Clin Pharmacol* **67**:421–426.
Spraggs CF, Budde LR, Briley LP, Bing N, Cox CJ, King KS, Whittaker JC, Mooser VE, Preston AJ, Stein SH, et al. (2011) HLA-DQA1*02:01 is a major risk factor for lapatinib-induced hepatotoxicity in women with advanced breast cancer. *J Clin Oncol* **29**:667–673.
Spraggs CF, Parham LR, Hunt CM, and Dollery CT (2012) Lapatinib-induced liver injury characterized by class II HLA and Gilbert's syndrome genotypes. *Clin Pharmacol Ther* **91**: 647–652.
Spraggs CF, Xu C-F, and Hunt CM (2013) Genetic characterization to improve interpretation and clinical management of hepatotoxicity caused by tyrosine kinase inhibitors. *Pharmacogenomics* **14**:541–554.
Takakusa H, Wahlin MD, Zhao C, Hanson KL, New LS, Chan ECY, and Nelson SD (2011) Metabolic intermediate complex formation of human cytochrome P450 3A4 by lapatinib. *Drug Metab Dispos* **39**:1022–1030.
Teng WC, Oh JW, New LS, Wahlin MD, Nelson SD, Ho HK, and Chan ECY (2010) Mechanism-based inactivation of cytochrome P450 3A4 by lapatinib. *Mol Pharmacol* **78**:693–703.
Teo YL, Saetaew M, Chanthawong S, Yap YS, Chan EC, Ho HK, and Chan A (2012) Effect of CYP3A4 inducer dexamethasone on hepatotoxicity of lapatinib: clinical and in vitro evidence. *Breast Cancer Res Treat* **133**:703–711.
Vuppugalla R and Mehvar R (2005) Enzyme-selective effects of nitric oxide on affinity and maximum velocity of various rat cytochromes P450. *Drug Metab Dispos* **33**:829–836.
Walsky RL, Obach RS, Hyland R, Kang P, Zhou S, West M, Geoghegan KF, Helal CJ, Walker GS, Goosen TC, et al. (2012) Selective mechanism-based inactivation of CYP3A4 by CYP3cide (PF-04981517) and its utility as an in vitro tool for delineating the relative roles of CYP3A4 versus CYP3A5 in the metabolism of drugs. *Drug Metab Dispos* **40**:1686–1697.
Wrighton SA, Brian WR, Sari MA, Iwasaki M, Guengerich FP, Raucy JL, Molowa DT, and Vandenbranden M (1990) Studies on the expression and metabolic capabilities of human liver cytochrome P450IIIA5 (HLp3). *Mol Pharmacol* **38**:207–213.
Yarden Y and Sliwkowski MX (2001) Untangling the ErbB signalling network. *Nat Rev Mol Cell Biol* **2**:127–137.

Address correspondence to: Dr. Klarissa D. Jackson, Department of Pharmaceutical Sciences, Lipscomb University College of Pharmacy and Health Sciences, One University Park Drive, Nashville, TN 37204. E-mail: klarissa.jackson@lipscomb.edu